On the Coexistence of Heterogeneous Services in 6G Networks: An Imperfection-aware RSMA Framework

Athanasios P. Chrysologou, *Graduate Student Member, IEEE,* Sotiris A. Tegos, *Senior Member, IEEE,* Panagiotis D. Diamantoulakis, *Senior Member, IEEE,* Nestor D. Chatzidiamantis, *Member, IEEE,* Paschalis C. Sofotasios, *Senior Member, IEEE,* and George K. Karagiannidis *Fellow, IEEE*

***Abstract*—One of the main challenges that the upcoming sixth-generation (6G) wireless networks will encounter is the necessity to design sophisticated multiple access techniques that besides being capable of supporting massive connectivity, they can also fulfill the heterogeneous requirements of 6G services, namely further-enhanced mobile broadband (feMBB), extremely reliable and low-latency communication, and ultra-massive machine-type communication (umMTC). To this end, this work investigates the coexistence of multiple feMBB and umMTC wireless sources in a network. In order to enhance the achievable connectivity, each orthogonal resource block of the network is assigned to one feMBB and multiple umMTC sources. FeMBB sources are assumed to constantly transmit, while umMTC are considered to access the network in a probabilistic manner. If more than one umMTC sources attempt to access the network in a given resource block, no umMTC transmission is permitted, however, when precisely one umMTC source endeavors to access the medium, rate-splitting multiple access is employed to concurrently serve both feMBB and umMTC transmissions. For such a communication scenario, we derive novel closed-form expressions for sources' outage probabilities (OPs), ergodic rates (ERs), system throughput, and ergodic sum rate under both the ideal case of perfect channel state information (pCSI) and perfect successive interference cancellation (pSIC) and the more realistic scenario of imperfect CSI (ipCSI) and imperfect SIC (ipSIC). Furthermore, a high signal-to-noise ratio analysis is provided revealing deeper insights for sources' asymptotic behavior under all considered cases. Simulation results corroborate the accuracy of the derived analytical expressions, investigate the impact of different system parameters on sources' OP and ER performance, and illustrate the detrimental impact of ipCSI and ipSIC on system performance compared to the ideal case of pCSI and pSIC.**

***Index Terms*—Rate-splitting multiple access (RSMA), network slicing, outage probability, ergodic rate, imperfect successive interference cancellation (SIC), imperfect channel state information (CSI).**

A. P. Chrysologou, S. A. Tegos, P. D. Diamantoulakis, and N. D. Chatzidiamantis are with the Department of Electrical and Computer Engineering, Aristotle University of Thessaloniki, 54124 Thessaloniki, Greece (e-mails: chrysolog@ece.auth.gr, tegosoti@auth.gr, padiaman@auth.gr, nestoras@auth.gr).

P. C. Sofotasios is with the C2PS and 6G Center, Department of Computer and Communications Engineering, Khalifa University, Abu Dhabi 127788, UAE. He is also with the Department of Electrical Engineering, Tampere University, FI-33101, Tampere, Finland (e-mail: paschalis.sofotasios@ku.ac.ae).

G. K. Karagiannidis is with the Wireless Communications and Information Processing Group (WCIP), Dept. of Electrical and Computer Engineering, Aristotle University of Thessaloniki, 54124 Thessaloniki, Greece and with the Cyber Security Systems and Applied AI Research Center, Lebanese American University (LAU), Lebanon (e-mail: geokarag@auth.gr).

The work of A. P. Chrysologou was supported by a PhD scholarship from the Bodossaki Foundation, Greece.

I. Introduction

The upcoming sixth-generation (6G) wireless communication systems are anticipated to address the escalating demands for increased data rates, enhanced reliability, ubiquitous and massive connectivity, and diverse levels of quality of experience (QoE) requirements [1], [2]. The fulfillment of these requirements is essential for meeting the needs of 6G types of services, including further-enhanced mobile broadband (feMBB), extremely reliable and low-latency communication (eRLLC), ultra massive machine-type communication (umMTC), as well as their combinations [3]. To effectively meet these stringent requirements, one of the fundamental necessities is the development of sophisticated multiple access schemes suitable for the next generation of wireless networks, referred to as next-generation multiple access [4], [5].

In this direction, rate-splitting multiple access (RSMA), first introduced in the late 1970s, has regained extensive research interest from both academia and industry because of its ability to provide a more general and robust transmission framework compared to non-orthogonal multiple access (NOMA) [6]–[8]. In downlink RSMA communication scenarios, the message intended for transmission is divided into two distinct parts known as the common message and the private message [9]. These components are individually encoded and transmitted using designated power levels for each part. Upon receiving the signal, the receiver decodes the common message first and subsequently subtracts it from the signal. This allows the receiver to decode its private message using successive interference cancellation (SIC) techniques. These pre-coding and post-coding processes represent a major step forward in realizing the concept of "intelligent joint transmitter-receiver interference management," which is considered to be a critical step in meeting the diverse requirements of 6G networks. On the other side, regarding the uplink scenario, users split their messages into multiple streams and allocate appropriate transmission power to each stream [9], [10]. Then, at the base station (BS), the receiver employs SIC to separate and retrieve each stream, ultimately reconstructing the original messages. Taking into account the significantly increased complexity levels of code construction and joint decoding at the receiver as well as the enhanced communication overhead and stringent synchronization demands that conventional methods, such as NOMA with joint decoding or NOMA with time sharing, require in order to achieve the capacity bound of the multiple

access channel (MAC), uplink RSMA with its basic principle of message splitting, can be viewed as low-complexity facilitator towards the achievement of every point of MAC capacity region [7].

A. Literature Review

A review of the open literature reveals that the majority of papers investigating RSMA focus on the downlink scenario. However, as explained, the use of RSMA for uplink data transmission theoretically has the potential to reach the capacity region of the MAC [9], [10]. In addition, given the critical importance of the uplink for numerous emerging 6G applications, such as augmented and virtual reality, connected robotics and autonomous systems, telemedicine, and more, the design and investigation of uplink multiple access techniques for next-generation networks becomes essential.

In [11], the outage as well as the achievable sum rate performance of a two-user uplink RSMA network was investigated. For a similar setup, [12] proved that both fairness and outage performance are improved by using rate splitting (RS) for a two-user uplink network. Compared to [11] and [12], which assumed a specific decoding order, in [13], the outage probability (OP) as well as the outage throughput for an uplink RSMA system model were derived under arbitrary decoding order and the benefits of the interplay between RSMA and slotted ALOHA were revealed. Taking into account the possible random nature of users' position inside a network, in [14], the outage performance of uplink RSMA transmissions when users are considered to be randomly deployed inside the network was studied taking both user scheduling schemes and power allocation strategies into consideration. Moreover, to leverage from the transmit diversity that cooperative transmissions achieve, in [15], a cooperative RSMA scheme was proposed and proven to offer enhanced performance levels compared to cooperative NOMA and cooperative orthogonal multiple access (OMA). An uplink NOMA-based network was considered in [16] and the use of a novel RS strategy capable of maximizing secondary user's achievable rate without affecting the outage performance of a primary user, was proposed. The superiority of the proposed scheme over existing benchmark schemes was demonstrated through simulations. Moreover, motivated by the advantages of NOMA in grant-free access, in [17], the use of RSMA in semi-grant-free (SGF) transmissions was attempted to further improve the outage performance of SGF schemes. In contrast to all previous contributions that mainly focused on outage performance or OP minimization in RSMA networks, in [18] two protocols based on RSMA and NOMA with SIC were presented and studied in terms of user's ergodic rate (ER). Useful insights were also provided, showing under what circumstances each protocol outperforms the other.

In the meantime, towards the enabling of massive connectivity while simultaneously satisfying all the heterogeneous needs and demands of eURRLC, feMBB, umMTC services, uplink RSMA has been proposed and investigated in terms of its ability to support network slicing, i.e., the division of the network into logical and physical sub-networks each tailored to specific demands such as latency, energy efficiency, mobility, massive connectivity, and throughput [19]–[22]. More specifically, in [19], the possible advantages of utilizing RSMA to support umMTC transmissions were pointed out, while in [20], the applicability of uplink RSMA to support the traffic generated by mMTC sources was investigated and the circumstances under which RSMA is beneficial were pointed out. In [21], an uplink RSMA-enabled network slicing approach was introduced for the simultaneous support of eMBB and URLLC services. It was revealed that RSMA was capable of achieving a larger capacity region compared to OMA and NOMA as soon as the power splitting factor is appropriately adjusted. In contrast to [21], which examined the eMBB and URLLC coexistence under the assumption that URLLC users have superior channel conditions compared to eMBB, [22] also analyzed the opposite scenario according to which an eMBB user experiences a better channel condition than a URLLC user and proved that the level of interference from the eMBB user directly influences the extent of improvements that can be achieved with RSMA. Furthermore, for the first time in the open literature, [22] investigated the RSMA-based coexistence of eMBB and mMTC.

B. Motivation and Contribution

Based on the aforementioned technical literature review and to the best of the authors' knowledge, it is observed that all existing works on uplink RSMA in the open literature assume perfect knowledge of channel state information (CSI). However, in practical scenarios, this assumption is idealistic and not applicable. In most real-world applications, receivers are not able to obtain perfect CSI (pCSI), leading to channel estimation errors (CEE) that create a notable impact on the overall system performance [23]–[25]. In the meantime, the successful implementation of non-orthogonal-based multiple access protocols, such as NOMA, RSMA, etc., also relies on effective SIC to mitigate interference. Previous works often assume that receivers can perfectly decode strong interfering signals and completely eliminate them from the received signal before decoding the desired signal. However, in practical systems, achieving accurate perfect SIC (pSIC) is not a straightforward task. Thus, practical applications are expected to frequently suffer from imperfect SIC (ipSIC), which would result in non-negligible performance degradation [26]–[28].

Considering the promising advantages of RSMA, the superior throughput performance of non-orthogonal-based multiple access protocols, as well as their ability to resolve collisions with the use of multi-user detection techniques, enabling higher connectivity levels [29], [30], it becomes necessary to investigate the performance of uplink RSMA under the common imperfections of ipSIC and imperfect CSI (ipCSI) encountered in realistic applications. Such a study would greatly assist RSMA system designers by providing useful theoretical and practical insights into the practical achievable performance and associated complexity. With this objective in mind, and taking into account the heterogeneous characteristics of all 6G services, we present and investigate an uplink communication scenario where multiple feMBB and umMTC wireless sources

harmoniously coexist in a network, all demanding to be served. In particular, the contributions of our work can be summarized as follows:

- We consider an uplink wireless network which consists of a BS and multiple feMBB and umMTC sources. Each feMBB source is assigned to occupy unique orthogonal resource blocks, e.g., unique time slots, while, in order to achieve enhanced connectivity levels, a number of umMTC sources is granted access to the resource blocks which would be solely occupied by each feMBB source. FeMBB sources transmit their messages in every time slot, while umMTC sources access the channel in a probabilistic manner. When more than one umMTC sources intent to access the network in a specific slot, then no umMTC transmission is allowed, while when exactly one of the umMTC sources attempts to access the medium, then uplink RSMA is utilized in order to simultaneously serve both feMBB and umMTC transmissions. For such a setup, we derive novel closed-form OP and ER expressions for the sources under the ideal assumption of pCSI and pSIC as well as under the more realistic scenario of ipCSI and ipSIC. Furthermore, the aforementioned mathematical expressions are utilized to derive closed-form expressions for the system overall outage throughput and ergodic sum rate (ESR). To the best of the authors' knowledge, analytical expressions for user OPs in an uplink RSMA system setup under the realistic assumption of ipCSI and ipSIC have not been extracted in the existing literature, while analytical ERs expressions have not been obtained for either the realistic case of ipCSI and ipSIC or the ideal case of pCSI and pSIC.
- To obtain further insights, asymptotic OP as well as ER analysis is carried out for the high signal-to-noise ratio (SNR) regime. Importantly, it is proven that, at high SNRs, OP floors appear for the sources under both pSIC, pCSI as well as ipCSI, ipSIC cases. On the other hand, when it comes to sources' ER, it is revealed that there are cases where ER floors can be avoided.
- Simulations and numerical results validate the authenticity of the presented analysis as well as illustrate the effect of different system parameters on the sources' OP, ER performance under all pCSI, pSIC, ipCSI, ipSIC cases. Furthermore, the detrimental impact of ipCSI and ipSIC on the sources' OP and ER as well as on the system throughput and ESR is revealed, thus dictating the need to include such practical constraints when studying RSMA-based systems.

C. Structure

The remainder of the paper is organized as follows: Section II describes the system model. In Section III, analytical OP as well as throughput expressions are derived, while in Section IV, an ER as well as an ESR analysis is provided. In Section V, simulation results are provided to authenticate the provided analytical results and to illustrate sources' and system's performance. Finally, Section VI concludes the paper.

II. System Model

We assume a wireless network which consists of a BS, $\mathcal{F}$ feMBB wireless sources and $\mathcal{N}$ umMTC wireless sources. It is assumed that all nodes are equipped with a single antenna and all sources intent to transmit their messages to the BS. In order to boost the achievable connectivity, we assume that each orthogonal resource block of the network is allocated to both a feMBB and multiple umMTC sources. Please note that FeMBB sources most commonly are bandwidth-hungry as well as delay-sensitive devices that demand increased reliability levels and high data rates. Hence, it is a common practice to let each feMBB source solely occupy orthogonal resource blocks [22]. However, this approach is highly inefficient for supporting massive connectivity as well as highly spectral-inefficient, which are two of the most of the most critical matters for 6G. In this context, also coinciding with the concept of non-orthogonal based network slicing, we propose that a number of umMTC sources is granted access to the resource blocks which would be solely occupied by a feMBB source. Therefore, the total number of $\mathcal{N}$ umMTC sources is divided into groups, where each group contains N_i sources, with $\sum_i N_i = \mathcal{N}$, and is allowed to share the unique orthogonal resource blocks which was initially assigned to a feMBB source.

Hereinafter, the analysis focuses on the interplay between one feMBB source, denoted as S_f, and a group of N umMTC sources, denoted as $\mathcal{U} = \{S_u^1, S_u^2, ..., S_u^N\}$, that share the same resource blocks, e.g., the same time slots. The channel coefficients between the sources and the BS are assumed to undergo Rayleigh fading, i.e., $h_i \sim \mathcal{CN}(0, \lambda_i)$ with $i \in \{S_f, S_u^1, ..., S_u^N\}$. Under ipCSI, according to minimum mean squared error (MMSE) estimation [23]–[25], it holds

$$h_i = \hat{h}_i + \epsilon_i, \tag{1}$$

where h_i is the actual channel, $\hat{h}_i$ is the estimate of h_i, and ϵ_i is the CEE, which is assumed to be complex normal random variable with zero mean and variance $\sigma_{\epsilon_i}^2$, i.e., $\epsilon_i \sim \mathcal{CN}(0, \sigma_{\epsilon_i}^2)$. Of note, the parameter $\sigma_{\epsilon_i}^2$ indicates the quality of channel estimation. Also, assuming that $\hat{h}_i$ and ϵ_i are uncorrelated [23], the estimated channel variance is given as $\hat{\lambda}_i = \lambda_i - \sigma_{\epsilon_i}^2$.

It is assumed that time is divided into time slots and that a number of time slots form a time frame. The feMBB source transmits its message in each time slot and is treated as a grant-based source. As a result, conventional frequent handshaking processes are performed between the feMBB source and the BS, during which the feMBB source informs the BS about its transmissions. On the other hand, a contention-based inspired access scheme is assumed for the umMTC sources. More specifically, at the beginning of each frame, the BS transmits a preamble packet to all umMTC sources. This packet serves the dual purpose of enabling frame synchronization and carrying information to the sources about the available slots within that frame. For each slot within the frame, each umMTC source independently determines whether to transmit or not in a stochastic manner, i.e., each umMTC source transmits in a particular time slot with probability p_u, where $u \in \mathcal{U}$. Note that the probability that a given number of umMTC sources

access the channel simultaneously is given by the product of N Bernoulli trials [31]. Note that the BS is informed how many umMTC sources intent to transmit at each slot within a frame during the handshake processes that precede the transmission processes [32].

Considering the above, from umMTC sources aspect, there are three distinct cases regarding the utilization of each time slot, namely i) no umMTC source attempts to access the channel, ii) precisely one of the umMTC sources intends to access the channel, and iii) two or more umMTC sources attempt to access the channel. In the first case, the feMBB source solely occupies the slot and performs OMA. In the third case, a collision occurs, i.e., no umMTC source is allowed to access the channel; thus, the feMBB source occupies the slot in a solely manner and performs OMA. On the other hand, in the second case, the umMTC source is granted access and shares the same slot with the feMBB source via uplink RSMA. At this point, it is important to note that the fact that no more than one umMTC source are allowed to access the channel simultaneously with the feMBB source is a practical, real-world driven assumption, since multi-user SIC detection requires long processing delays, high complexity, and is subject to SIC propagation errors. Furthermore, consider that a network has many orthogonal resources; thus, multiple groups consisting of one feMBB and multiple umMTC sources are served simultaneously within the network. Moreover, note that in conventional OMA-based network slicing approaches, where umMTC services do not share their resources with feMBB services and access the network via conventional random access protocols such as slotted ALOHA, collisions result in unused resources [30]. In contrast, in our proposed access scheme, when a collision occurs between umMTC sources, the orthogonal resource block does not remain unused because it always serves a feMBB source. Moreover, compared to conventional OMA-based network slicing approaches, where only a portion of the available network resources are allocated to umMTC services, we allow umMTC sources to access all network resources, so that the critical demand for enhanced umMTC connectivity could be met through careful interference management.

From the above, it becomes evident that it is the heterogeneous characteristics of feMBB and umMTC services, i.e., the high data traffic loads that require constant transmissions in every slot and the large number of sources that access the medium in a probabilistic manner, respectively, that create the need to develop a hybrid OMA-RSMA access scheme. In this context, it occurs that with probability

$$q = \sum_{u \in \mathcal{U}} p_u \prod_{\substack{n \in \mathcal{U}, \\ n \neq u}} (1 - p_n), \tag{2}$$

exactly one out of the N umMTC sources attempts to access the wireless medium and, thus, will share the time slot with the feMBB source, while with probability $(1-q)$ none or more than one umMTC sources intent to access the medium, and thus, the feMBB will be the unique source that accesses the channel via OMA. From (2), it occurs that umMTC sources' access probabilities p_u as well as their total number N are really important design parameters since they define the frequency with which the feMBB source accesses the medium alone or shares the wireless channel with a umMTC source. With probability $(1-q)$, the message received at the BS can be written as

$$y_B^I = \sqrt{P}\hat{h}_f x_f + n_b, \tag{3}$$

where x_f is feMBB source's message, P is sources' transmit power, and n_b stands for the additive white Gaussian noise (AWGN) with zero mean and variance N_0 at the BS. Furthermore, considering ipCSI, the received SINR at the BS for the decoding of x_f can be extracted by invoking (1) in (3) as

$$\gamma_{x_f}^{\text{OMA}} = \frac{\rho|\hat{h}_f|^2}{\rho\sigma_{\epsilon_f}^2 + 1}, \tag{4}$$

where $\rho = \frac{P}{N_0}$ is sources' transmit SNR whilst the first term of the denominator occurs due to the ipCSI.

On the contrary, with probability q, a umMTC source accesses the network using the same resources with the feMBB source, i.e., in a non-orthogonal manner. In this context, uplink RSMA is used in the present contribution to enable sources' non-orthogonal transmissions. In uplink RSMA, the message of only one source needs to be split to achieve the capacity region [11]. Hence, denoting as S_u the umMTC source that is allowed to transmit alongside the feMBB source, it is assumed that only S_u splits its message and therefore, the message received at the BS can be expressed as

$$y_B^{II} = \sqrt{a_1 P}h_u x_{u1} + \sqrt{a_2 P}h_u x_{u2} + \sqrt{P}h_f x_f + n_b, \tag{5}$$

where x_{u1}, x_{u2} are the two parts of S_u's message and a_1, a_2 are the power allocation coefficients for x_{u1}, x_{u2}, respectively, with $a_1 + a_2 = 1$. At this point, it is important to note that the fact that S_u, instead of S_f, splits its message leads to reduced coordination complexity.[1] In particular, when S_f performs OMA, there is clearly no reason to split its message. Thus, assuming that S_f splits its message during RSMA would lead to increased coordination complexity as well as to time-consuming pre-transmission processes during which, when the BS is informed that a umMTC source will access the channel, it then notifies S_f to stop transmitting its message in an unsplit manner and to start performing message splitting.

It has been proven that the decoding order that allows uplink RSMA to reach the capacity region is (x_{u1}, x_f, x_{u2}) under all channel states [11], [12]. Hence, invoking (1) in (5), the received signal-to-interference-plus-noise ratio (SINR) at the BS for the detection of message x_{u1}, can be modeled as

$$\gamma_{x_{u1}} = \frac{a_1\rho|\hat{h}_u|^2}{\rho\sigma_{\epsilon_u}^2 + \rho|\hat{h}_f|^2 + \rho\sigma_{\epsilon_f}^2 + a_2\rho|\hat{h}_u|^2 + 1}. \tag{6}$$

According to the pSIC case, having successfully decoded x_{u1} and exploiting the channel estimation $\hat{h}_u$, the BS is capable of generating the term $\sqrt{a_1 P}\hat{h}_u x_{u1}$ and perfectly removing it

[1]It is further noted that the performance analysis of the RSMA framework provided in the following sections is generalized and applicable at all cases where two sources perform uplink RSMA. Hence, the analysis can be readily extended to the case when S_f instead of S_u performs RS.

from the received y_B^{II} presented in (5). Conversely, assuming ipSIC, the aforementioned term is not completely removed from (5) and, thus, the decoding of x_f is attempted in the presence of residual interference due to ipSIC. In a similar manner, the decoding of x_{u2} is attempted in the presence of residual interference caused by the incomplete elimination of $\sqrt{a_1 P}\hat{h}_u x_{u1}$ and $\sqrt{P}\hat{h}_f x_f$ from (5). Hence, the received SINRs at the BS for the detection of messages x_f and x_{u2} can be respectively modeled as

$$\gamma_{x_f,u} = \frac{\rho|\hat{h}_f|^2}{\rho\sigma_{\epsilon_f}^2 + \rho\sigma_{\epsilon_u}^2 + a_2\rho|\hat{h}_u|^2 + \tilde{k}_1 a_1 \rho|\hat{h}_u|^2 + 1}, \quad (7)$$

$$\gamma_{x_{12}} = \frac{a_2\rho|\hat{h}_u|^2}{\rho\sigma_{\epsilon_u}^2 + \tilde{k}_1 a_1 \rho|\hat{h}_u|^2 + \tilde{k}_2\rho|\hat{h}_f|^2 + \rho\sigma_{\epsilon_f}^2 + 1}, \quad (8)$$

where $\tilde{k}_1$, $\tilde{k}_2$ quantify the impact of ipSIC. It is mentioned that $\tilde{k}_j \in [0,1]$ with $\tilde{k}_j = 0$ denoting pSIC and $\tilde{k}_j = 1$ denoting the no SIC case.

It is noted that, to the best of authors' knowledge, there is no existing contribution that studies uplink RSMA under the practical assumptions of ipCSI and ipSIC. Hence, (6)-(8) appear for the first time in the open literature. Furthermore, given the fact that NOMA can be viewed as a special case of RSMA [6], [7], it is ensured that, via appropriate power allocation and RS parameter selection, the proposed OMA-RSMA scheme outperforms conventional OMA-NOMA approaches.

III. Outage & Throughput Analysis

Capitalizing on the above, this section presents the derivation of analytical expressions for the OPs of all messages, since OP constitutes a meaningful performance evaluation metric for applications where users transmit with constant data rates. An outage occurs when corresponding SINR falls below a predefined threshold, which, for the examined system setup, can be given as $r_{u1} = 2^{\beta_u R_u} - 1$, $r_f = 2^{R_f} - 1$ and $r_{u2} = 2^{(1-\beta_u)R_u} - 1$ for messages x_{u1}, x_f and x_{u2}, respectively, where R_u and R_f are S_u's, S_f's target data rates, respectively, $\beta_u \in [0,1]$ denotes the target rate factor [13] and $u \in \mathcal{U}$.

A. OP of x_{u1}

Assuming that S_u accesses the channel, then given the fact that x_{u1} is decoded first at the BS, its OP can be evaluated as

$$P_{u1}^o = \Pr\left(\gamma_{x_{u1}} < r_{u1}\right). \quad (9)$$

The following theorem provides x_{u1}'s OP under ipCSI.

Theorem 1. *When S_u accesses the channel, the OP of message x_{u1} under ipCSI can be evaluated as*

$$P_{u1}^o = \begin{cases} 1 - \frac{\hat{\lambda}_u(a_1 - a_2 r_{u1})}{\tilde{\lambda}_u(a_1 - a_2 r_{u1}) + \hat{\lambda}_f r_{u1}} e^{-\frac{D_1 r_{u1}}{\tilde{\lambda}_u \rho(a_1 - a_2 r_{u1})}}, & \frac{a_1}{a_2} > r_{u1} \\ 1, & \text{otherwise,} \end{cases} \quad (10)$$

where $D_1 = \rho\sigma_{\epsilon_u}^2 + \rho\sigma_{\epsilon_f}^2 + 1$.

Proof: By invoking (6) in (9), we obtain

$$\begin{aligned} P_{u1}^o &= \Pr\left(\frac{a_1\rho|\hat{h}_u|^2}{\rho|\hat{h}_f|^2 + a_2\rho|\hat{h}_u|^2 + D_1} < r_{u1}\right) \\ &= \begin{cases} \Pr\left(|\hat{h}_u|^2 < \frac{\rho|\hat{h}_f|^2 r_{u1} + D_1 r_{u1}}{a_1\rho - a_2\rho r_{u1}}\right), & \frac{a_1}{a_2} > r_{u1} \\ 1, & \text{otherwise.} \end{cases} \end{aligned} \quad (11)$$

Focusing on the case when $\frac{a_1}{a_2} > r_{u1}$, it follows that

$$\begin{aligned} P_{u1}^o &= \int_0^\infty F_{|\hat{h}_u|^2}\left(\frac{\rho r_{u1} y + D_1 r_{u1}}{a_1\rho - a_2\rho r_{u1}}\right) f_{|\hat{h}_f|^2}(y)\,\mathrm{d}y \\ &= 1 - \frac{1}{\hat{\lambda}_f} e^{-\frac{D_1 r_{u1}}{\tilde{\lambda}_u\rho(a_1 - a_2 r_{u1})}} \int_0^\infty e^{-y\left(\frac{1}{\hat{\lambda}_f} + \frac{r_{u1}}{\tilde{\lambda}_u(a_1 - a_2 r_{u1})}\right)} \mathrm{d}y, \end{aligned} \quad (12)$$

where $F_Z(\cdot)$, $f_Z(\cdot)$ denote the cumulative distribution function (CDF) and probability density function (PDF), respectively, of a random variable (RV) Z. By performing the exponential integration of (12) and after some basic algebraic manipulations, (10) is derived, which concludes the proof. ∎

Remark 1. *Given that x_{u1} is decoded first at the BS, its outage performance is not affected from ipSIC. On the other hand, the OP of message x_{u1} under pCSI can be given via (10) by setting parameters $\sigma_{\epsilon_u}^2$, $\sigma_{\epsilon_f}^2$ equal to zero.*

B. OP of x_f

When it comes to S_f, two cases must be taken into consideration, namely i) only S_f accesses the channel, and ii) S_f shares the channel with a umMTC source, denoted as S_u. For the first case, x_f's OP can be given as

$$P_f^{\text{OMA}} = \Pr\left(\gamma_{x_f}^{\text{OMA}} < r_f\right). \quad (13)$$

In the second case, in order to avoid outage for x_f, the BS has to successfully decode x_{u1} and then attempt to decode x_f via SIC. Hence,

$$P_{f,u}^{\text{RSMA}} = 1 - \Pr\left(\gamma_{x_{u1}} > r_{u1}, \gamma_{x_f,u} > u_f\right). \quad (14)$$

The following theorem provides the OP of x_f under ipCSI and ipSIC.

Theorem 2. *The OP of message x_f under ipCSI and ipSIC can be evaluated as*

$$P_{f,u}^o = (1-q)\left(1 - e^{-\frac{r_f D_2}{\hat{\lambda}_f \rho}}\right) + \sum_{u\in\mathcal{U}} p_u P_{f,u}^{\text{RSMA}} \prod_{\substack{n\in\mathcal{U}, \\ n\neq u}} (1-p_n), \quad (15)$$

where $D_2 = \rho\sigma_{\epsilon_f}^2 + 1$, $P_{f,u}^{\text{RSMA}}$ is given by (16) at the top of the next page, with condition Δ_1 being defined as

$$\Delta_1 : \{r_{u1}(a_2 r_f + \tilde{k}_1 a_1 r_f) - a_1 + a_2 r_{u1} < 0\} \quad (17)$$

and

$$A = \frac{D_1 u_f(a_1 - a_2 r_{u1}) - D_1 r_{u1}(a_2 u_f + \tilde{k}_1 a_1 u_f)}{\rho r_{u1}(a_2 u_f + \tilde{k}_1 a_1 u_f) - \rho(a_1 - a_2 r_{u1})}. \quad (18)$$

Proof: The proof is provided in Appendix A. ∎

$$P_{f,u}^{\text{RSMA}} = \begin{cases} 1 - \frac{1}{1+\frac{\bar{\lambda}_f r_{u1}}{\bar{\lambda}_u \rho (a_1 - a_2 r_{u1})}} e^{-\frac{D_1 r_{u1}}{\bar{\lambda}_u \rho (a_1 - a_2 r_{u1})} - \left(\frac{1}{\bar{\lambda}_f} + \frac{r_{u1}}{\bar{\lambda}_u (a_1 - a_2 r_{u1})}\right) A} \\ \quad + \frac{1}{1+\frac{\bar{\lambda}_f}{\bar{\lambda}_u (a_2 r_f + \tilde{k}_1 a_1 u_f)}} e^{\frac{D_1 r_f}{\bar{\lambda}_u \rho (a_2 r_f + \tilde{k}_1 a_1 r_f)} - \left(\frac{1}{\bar{\lambda}_f} + \frac{1}{\bar{\lambda}_u (a_2 r_f + \tilde{k}_1 a_1 r_f)}\right) A}, & \frac{a_1}{a_2} > r_{u1} \ \& \ \Delta_1 \\ 0, & \text{otherwise} \end{cases} \tag{16}$$

Remark 2. *The OP of message x_f under pSIC can be evaluated via (15) by setting $\tilde{k}_1$ equal to zero. Likewise, the OP of message x_f under pCSI can be evaluated via (15) as soon as parameters $\sigma_{\epsilon_u}^2$, $\sigma_{\epsilon_f}^2$ are set equal to zero.*

It is noted that condition Δ_1 can be seen as an "operation-condition", i.e., if it does not hold then S_f faces a constant outage. Hence, power allocation factors a_1, a_2 must be carefully determined since these parameters directly affect Δ_1. Furthermore, it can be observed that (15) consists of two terms. The first term refers to the OMA case and is multiplied by the probability that OMA is used for S_f's access. The second term refers to the RSMA case and is multiplied by the probability that RSMA is utilized. The probabilities that refer to the OMA, RSMA case, as also (2) dictates, are heavily affected from the total number N of umMTC sources that are grouped with the feMBB source as well as from the umMTC sources' access probability p_u. Hence, these parameters heavily affect which of the OMA or RSMA term is the dominant in (15), and thus, determine the S_f's overall outage performance.

C. OP of x_{u2}

When S_u accesses the channel and in order to avoid outage for x_{u2}, the BS has to successfully decode x_{u1} and x_f and then attempt to decode x_{u2} via SIC. Hence, it holds

$$P_{u2}^{o} = 1 - \Pr\left(\gamma_{x_{u1}} > r_{u1}, \gamma_{x_f,u} > r_f, \gamma_{x_{u2}} > r_{u2}\right). \tag{19}$$

The following theorem returns the OP of x_{u2} under ipCSI and ipSIC.

Theorem 3. *When S_u accesses the channel, the OP of message x_{u2} under ipCSI and ipSIC can be evaluated as*

$$P_{u2}^{o} = \begin{cases} 1 - P_{u2}^{A} - P_{u2}^{B}, & \frac{a_1}{a_2} > r_{u1} \ \& \ \frac{a_2}{\tilde{k}_1 a_1} > r_{u2} \\ 1, & \text{otherwise,} \end{cases} \tag{20}$$

where P_{r2}^{A} and P_{r2}^{B} are given in Table I with

$$Q = -\frac{D_1 r_f (a_2 - \tilde{k}_1 a_1 r_{u2}) + D_1 r_{u2}(a_2 r_f + \tilde{k}_1 a_1 r_f)}{\tilde{k}_2 r_{u2}(a_2 \rho r_f + \tilde{k}_1 a_1 \rho r_f) - a_2 \rho + \tilde{k}_1 a_1 \rho r_{u2}}, \tag{21}$$

$$C_1 = \frac{r_{u1}}{a_1 - a_2 r_{u1}} - \frac{\tilde{k}_2 r_{u2}}{a_2 - \tilde{k}_1 a_1 r_{u2}}, \tag{22}$$

$$C_2 = \frac{D_1 r_{u2}}{a_2 \rho - \tilde{k}_1 a_1 \rho r_{u2}} - \frac{D_1 r_{u1}}{a_1 \rho - a_2 \rho r_{u1}}. \tag{23}$$

Proof: Invoking (6), (7) and (8) in (19) and performing some algebraic manipulations, we get

$$P_{u2}^{o} = \begin{cases} 1 - P_{u2,1}^{o}, & \frac{a_1}{a_2} > r_{u1} \ \& \ \frac{a_2}{\tilde{k}_1 a_1} > r_{u2} \\ 1, & \text{otherwise,} \end{cases} \tag{24}$$

where

$$P_{u2,1}^{o} = \Pr\Bigg(|\hat{h}_u|^2 > \frac{\rho|\hat{h}_f|^2 r_{u1} + D_1 r_{u1}}{a_1 \rho - a_2 \rho r_{u1}}, \\ |\hat{h}_u|^2 < \frac{\rho|\hat{h}_f|^2 - D_1 r_f}{a_2 \rho r_f + \tilde{k}_1 a_1 \rho r_f}, |\hat{h}_u|^2 > \frac{\tilde{k}_2 \rho |\hat{h}_f|^2 r_{u2} + D_1 r_{u2}}{a_2 \rho - \tilde{k}_1 a_1 \rho r_{u2}}\Bigg). \tag{25}$$

Given that the events that appear in (25) contain the same RVs, its calculation is far from a straightforward task since it consists of multiple non-independent events. In this context, in order to further proceed into the calculation of the probability of (25), we must first determine for which $|\hat{h}_f|^2$ values the following inequalities hold

$$\frac{\rho|\hat{h}_f|^2 r_{u1} + D_1 r_{u1}}{a_1 \rho - a_2 \rho r_{u1}} > \frac{\tilde{k}_2 \rho |\hat{h}_f|^2 r_{u2} + D_1 r_{u2}}{a_2 \rho - \tilde{k}_1 a_1 \rho r_{u2}}, \tag{26}$$

$$\frac{\rho|\hat{h}_f|^2 r_{u1} + D_1 r_{u1}}{a_1 \rho - a_2 \rho r_{u1}} < \frac{\tilde{k}_2 \rho |\hat{h}_f|^2 r_{u2} + D_1 r_{u2}}{a_2 \rho - \tilde{k}_1 a_1 \rho r_{u2}}. \tag{27}$$

After some manipulations, (26) can be transformed into

$$C_1 |\hat{h}_f|^2 > C_2, \tag{28}$$

where C_1, C_2 are given via (22), (23), respectively.

It is evident that when $C_1 > 0$ and $C_2 < 0$, then (26) always holds while (27) never holds. Conversely, when $C_1 < 0$ and $C_2 > 0$, then (26) never holds while (27) always holds. On the other hand, when $C_1, C_2 > 0$, then (26) holds when $|\hat{h}_f|^2 > \frac{C_2}{C_1}$, while (27) holds when $|\hat{h}_f|^2 < \frac{C_2}{C_1}$. Finally, when $C_1, C_2 < 0$, then (26) holds when $|\hat{h}_f|^2 < \frac{C_2}{C_1}$, while (27) holds when $|\hat{h}_f|^2 > \frac{C_2}{C_1}$. Considering all the above, $P_{u2,1}^{o}$ can be given via (29) at the top of page 8.

By evaluating the probabilities of (29) in a similar manner as in (58) given in Appendix A, it occurs that P_{u2}^{o} is given by (20), which concludes the proof. ∎

Remark 3. *The OP of message x_{u2} under pSIC can be evaluated via (20) by setting $\tilde{k}_1$, $\tilde{k}_2$ equal to zero. Likewise, the OP of message x_{u2} under pCSI can be evaluated via (20) as soon as parameters $\sigma_{\epsilon_u}^2$, $\sigma_{\epsilon_f}^2$ are set equal to zero.*

D. Asymptotic outage behavior

In this section, the sources' outage performance at the high SNR regime is investigated.

Lemma 1. *At the high SNR regime and under ipCSI and ipSIC, all x_{u1}, x_f and x_{u2} messages show outage floors which can be given via (10), (15) and (20), respectively, by replacing D_j with $\tilde{D}_j = D_j - 1$, where $j \in \{1, 2\}$.*

TABLE I: P_{u2}^{A}, P_{u2}^{B}

Term	Conditions		Expression
P_{u2}^{A}	$r_{u1}(a_2r_f+\tilde{k}_1a_1r_f)-a_1+a_2r_{u1}<0$	$C_1>0$ $C_2<0$	$\frac{1}{1+\frac{\hat{\lambda}_f r_{u1}}{\hat{\lambda}_u(a_1-a_2r_{u1})}}e^{-\frac{D_1r_{u1}}{\hat{\lambda}_u\rho(a_1-a_2r_{u1})}-\left(\frac{1}{\hat{\lambda}_f}+\frac{r_{u1}}{\hat{\lambda}_u(a_1-a_2r_{u1})}\right)A}$ $-\frac{1}{1+\frac{\hat{\lambda}_f}{\hat{\lambda}_u(a_2r_f+\tilde{k}_1a_1r_f)}}e^{\frac{D_1r_f}{\hat{\lambda}_u\rho(a_2r_f+\tilde{k}_1a_1r_f)}-\left(\frac{1}{\hat{\lambda}_f}+\frac{1}{\hat{\lambda}_u(a_2r_f+\tilde{k}_1a_1r_f)}\right)A}$
		$C_1>0$ $C_2>0$	$\frac{1}{1+\frac{\hat{\lambda}_f r_{u1}}{\hat{\lambda}_u(a_1-a_2r_{u1})}}e^{-\frac{D_1r_{u1}}{\hat{\lambda}_u\rho(a_1-a_2r_{u1})}-\left(\frac{1}{\hat{\lambda}_f}+\frac{r_{u1}}{\hat{\lambda}_u(a_1-a_2r_{u1})}\right)\max\left\{A,\frac{C_2}{C_1}\right\}}$ $-\frac{1}{1+\frac{\hat{\lambda}_f}{\hat{\lambda}_u(a_2r_f+\tilde{k}_1a_1r_f)}}e^{\frac{D_1r_f}{\hat{\lambda}_u\rho(a_2r_f+\tilde{k}_1a_1r_f)}-\left(\frac{1}{\hat{\lambda}_f}+\frac{1}{\hat{\lambda}_u(a_2u_2+\tilde{k}_1a_1r_f)}\right)\max\left\{A,\frac{C_2}{C_1}\right\}}$
		$C_1<0$ $C_2<0$ $A<\frac{C_2}{C_1}$	$\frac{1}{1+\frac{\hat{\lambda}_f r_{u1}}{\hat{\lambda}_u(a_1-a_2r_{u1})}}e^{-\frac{D_1r_{u1}}{\hat{\lambda}_u\rho(a_1-a_2r_{u1})}}\left(e^{-\left(\frac{1}{\hat{\lambda}_f}+\frac{r_{u1}}{\hat{\lambda}_u(a_1-a_2r_{u1})}\right)A}-e^{-\left(\frac{1}{\hat{\lambda}_f}+\frac{r_{u1}}{\hat{\lambda}_u(a_1-a_2r_{u1})}\right)\frac{C_2}{C_1}}\right)$ $-\frac{1}{1+\frac{\hat{\lambda}_f}{\hat{\lambda}_u(a_2u_2+\tilde{k}_1a_1r_f)}}e^{\frac{D_1r_f}{\hat{\lambda}_u\rho(a_2r_f+\tilde{k}_1a_1r_f)}}\left(e^{-\left(\frac{1}{\hat{\lambda}_f}+\frac{1}{\hat{\lambda}_u(a_2r_f+\tilde{k}_1a_1r_f)}\right)A}-e^{-\left(\frac{1}{\hat{\lambda}_f}+\frac{1}{\hat{\lambda}_u(a_2r_f+\tilde{k}_1a_1r_f)}\right)\frac{C_2}{C_1}}\right)$
	otherwise		0
P_{u2}^{B}	$\tilde{k}_2r_{u2}(a_2r_f+\tilde{k}_1a_1r_f)-a_2+\tilde{k}_1a_1r_{u2}<0$	$C_1>0$ $C_2>0$ $Q<\frac{C_2}{C_1}$	$\frac{1}{1+\frac{\hat{\lambda}_f\rho r_{u2}}{\hat{\lambda}_u(a_2\rho-\tilde{k}_1a_1\rho r_{u2})}}e^{-\frac{D_1r_{u2}}{\hat{\lambda}_u(a_2\rho-\tilde{k}_1a_1\rho r_{u2})}}\left(e^{-\left(\frac{1}{\hat{\lambda}_f}+\frac{\tilde{k}_2\rho r_{u2}}{\hat{\lambda}_u(a_2\rho-\tilde{k}_1a_1\rho r_{u2})}\right)Q}-e^{-\left(\frac{1}{\hat{\lambda}_f}+\frac{\tilde{k}_2\rho r_{u2}}{\hat{\lambda}_u(a_2\rho-\tilde{k}_1a_1\rho r_{u2})}\right)\frac{C_2}{C_1}}\right)$ $-\frac{1}{1+\frac{\hat{\lambda}_f\rho}{\hat{\lambda}_u(a_2\rho r_f+\tilde{k}_1a_1\rho r_f)}}e^{\frac{D_1r_f}{\hat{\lambda}_u\rho(a_2r_f+\tilde{k}_1a_1r_f)}}\left(e^{-\left(\frac{1}{\hat{\lambda}_f}+\frac{\rho}{\hat{\lambda}_u(a_2\rho r_f+\tilde{k}_1a_1\rho r_f)}\right)Q}-e^{-\left(\frac{1}{\hat{\lambda}_f}+\frac{\rho}{\hat{\lambda}_u(a_2\rho u_2+\tilde{k}_1a_1\rho r_f)}\right)\frac{C_2}{C_1}}\right)$
		$C_1<0$ $C_2<0$	$\frac{1}{1+\frac{\hat{\lambda}_f\rho r_{u2}}{\hat{\lambda}_u(a_2\rho-\tilde{k}_1a_1\rho r_{u2})}}e^{-\frac{D_1r_{u2}}{\hat{\lambda}_u(a_2\rho-\tilde{k}_1a_1\rho r_{u2})}-\left(\frac{1}{\hat{\lambda}_f}+\frac{\tilde{k}_2\rho r_{u2}}{\hat{\lambda}_u(a_2\rho-\tilde{k}_1a_1\rho r_{u2})}\right)\max\left\{Q,\frac{C_2}{C_1}\right\}}$ $-\frac{1}{1+\frac{\hat{\lambda}_f\rho}{\hat{\lambda}_u(a_2\rho r_f+\tilde{k}_1a_1\rho r_f)}}e^{\frac{D_1r_f}{\hat{\lambda}_u\rho(a_2r_f+\tilde{k}_1a_1r_f)}-\left(\frac{1}{\hat{\lambda}_f}+\frac{\rho}{\hat{\lambda}_u(a_2\rho r_f+\tilde{k}_1a_1\rho r_f)}\right)\max\left\{Q,\frac{C_2}{C_1}\right\}}$
		$C_1<0$ $C_2>0$	$\frac{1}{1+\frac{\hat{\lambda}_f\rho r_{u2}}{\hat{\lambda}_u(a_2\rho-\tilde{k}_1a_1\rho r_{u2})}}e^{-\frac{D_1r_{u2}}{\hat{\lambda}_u(a_2\rho-\tilde{k}_1a_1\rho r_{u2})}-\left(\frac{1}{\hat{\lambda}_f}+\frac{\tilde{k}_2\rho r_{u2}}{\hat{\lambda}_u(a_2\rho-\tilde{k}_1a_1\rho r_{u2})}\right)Q}$ $-\frac{1}{1+\frac{\hat{\lambda}_f\rho}{\hat{\lambda}_u(a_2\rho u_2+\tilde{k}_1a_1\rho r_f)}}e^{\frac{D_1r_f}{\hat{\lambda}_u\rho(a_2r_f+\tilde{k}_1a_1r_f)}-\left(\frac{1}{\hat{\lambda}_f}+\frac{\rho}{\hat{\lambda}_u(a_2\rho r_f+\tilde{k}_1a_1\rho r_f)}\right)Q}$
	otherwise		0

Proof: In (10), (15) and (20), it can be observed that the arguments of the exponential functions have the form:

$$\frac{GD_j}{B\rho}=\frac{G(D_j-1)+G}{B\rho}, \tag{30}$$

where $j\in\{1,2\}$ and G, B are positive constants. It is noted that (D_j-1) has the form of $(D_j-1)=N_j\rho$, with N_j being a positive constant for every $j\in\{1,2\}$.

By further taking into account that, at the high SNR regime, i.e., for $\rho\to\infty$ values, $G(D_j-1)+G\approx G(D_j-1)$, it follows that

$$\frac{G(D_j-1)+G}{B\rho}\approx\frac{G(D_j-1)}{B\rho},\quad \text{when } \rho\to\infty. \tag{31}$$

Taking into account that the term $\frac{G(D_j-1)}{B\rho}=\frac{GN_j\rho}{B\rho}=\frac{GN_j}{B}$ is a constant value which does not depend on ρ, it can be concluded that, at the high SNR regime, the OPs of all messages show a constant outage floor, which concludes the proof. ■

Remark 4. *For the case of ipCSI and pSIC, the asymptotic expressions provided in Lemma 1 still hold as soon as $\tilde{k}_1$, $\tilde{k}_2$ are set equal to zero. On the other hand, for the case of pCSI (and pSIC or ipSIC), the arguments of the exponential functions in (10), (15) and (20) have the form of $\frac{G}{B\rho}$. Hence, applying the approximation $e_{x\to0}(-x)\approx1-x$ and taking the limit when $\rho\to\infty$ then it occurs that at high SNR regime, the OPs of all messages also exhibit outage floors.*

Remark 5. *From the above lemma, it becomes obvious that OP floors of the messages are directly affected from the ipCSI and ipSIC parameters.*

E. Throughput analysis

Utilizing the OP expressions provided in the previous section, the throughput of S_f and S_u, as well as umMTC sources' sum throughput and system's overall sum throughput can be evaluated.

Theorem 4. *The throughput of S_f and S_u, with $u\in\mathcal{U}$, are*

$$P_{u2,1}^{o}=\begin{cases}\Pr\left(\frac{\rho|\hat{h}_f|^2r_{u1}+D_1r_{u1}}{a_1\rho-a_2\rho r_{u1}}<|\hat{h}_u|^2<\frac{\rho|\hat{h}_f|^2-D_1r_f}{a_2\rho r_f+\tilde{k}_1a_1\rho r_f}\right), & C_1>0,C_2<0\\ \Pr\left(\frac{\tilde{k}_2\rho|\hat{h}_f|^2r_{u2}+D_1r_{u2}}{a_2\rho-\tilde{k}_1a_1\rho r_{u2}}<|\hat{h}_u|^2<\frac{\rho|\hat{h}_f|^2-D_1r_f}{a_2\rho r_f+\tilde{k}_1a_1\rho r_f}\right), & C_1<0,C_2>0\\ \Pr\left(\frac{\rho|\hat{h}_f|^2r_{u1}+D_1r_{u1}}{a_1\rho-a_2\rho r_{u1}}<|\hat{h}_u|^2<\frac{\rho|\hat{h}_f|^2-D_1r_f}{a_2\rho r_f+\tilde{k}_1a_1\rho r_f},|\hat{h}_f|^2>\frac{C_2}{C_1}\right)\\ \quad+\Pr\left(\frac{\tilde{k}_2\rho|\hat{h}_f|^2r_{u2}+D_1ru2}{a_2\rho-\tilde{k}_1a_1\rho r_{u2}}<|\hat{h}_u|^2<\frac{\rho|\hat{h}_f|^2-D_1r_f}{a_2\rho r_f+\tilde{k}_1a_1\rho r_f},|\hat{h}_f|^2<\frac{C_2}{C_1}\right), & C_1,C_2>0\\ \Pr\left(\frac{\rho|\hat{h}_f|^2r_{u1}+D_1r_{u1}}{a_1\rho-a_2\rho r_{u1}}<|\hat{h}_u|^2<\frac{\rho|\hat{h}_f|^2-D_1r_f}{a_2\rho r_f+\tilde{k}_1a_1\rho r_f},|\hat{h}_f|^2<\frac{C_2}{C_1}\right)\\ \quad+\Pr\left(\frac{\tilde{k}_2\rho|\hat{h}_f|^2r_{u2}+D_1ru2}{a_2\rho-\tilde{k}_1a_1\rho r_{u2}}<|\hat{h}_u|^2<\frac{\rho|\hat{h}_f|^2-D_1r_f}{a_2\rho r_f+\tilde{k}_1a_1\rho r_f},|\hat{h}_f|^2>\frac{C_2}{C_1}\right), & C_1,C_2<0\end{cases}\tag{29}$$

given via (32) and (33), respectively. Furthermore, umMTC sources' sum throughput as well as system's overall sum throughput are provided via (34) and (35), respectively.

$$T_f=(1-q)\left(1-P_f^{\text{OMA}}\right)R_f+R_f\sum_{u\in\mathcal{U}}p_u\left(1-P_{f,u}^{\text{RSMA}}\right)\prod_{\substack{n\in\mathcal{U},\\ n\neq u}}(1-p_n)\tag{32}$$

$$T_u=p_u\left((1-P_{u1}^{o})\beta R_u+(1-P_{u2}^{o})(1-\beta)R_u\right)\prod_{\substack{n\in\mathcal{U},\\ n\neq u}}(1-p_n)\tag{33}$$

$$T_{\mathcal{U}}=\sum_{u\in\mathcal{U}}T_u\tag{34}$$

$$T_{sum}=T_f+T_{\mathcal{U}}\tag{35}$$

Proof: It is pointed out that, with probability $(1-q)$, S_f is the only source that accesses the channel, i.e., its OP can be determined by (55). On the other hand, with probability $p_u\prod_{\substack{n\in\mathcal{U},\\ n\neq u}}(1-p_n)$, S_f shares the channel with the u-th umMTC source, thus S_f's OP can be given via (16), while, the OPs of S_u's substreams x_{u1} and x_{u2} can be calculated via (10) and (20), respectively. Taking into account the above observations, (32)-(35) can be readily deduced. ■

IV. Ergodic Rate Analysis

In scenarios where source's target data rate is dynamically changed depending on source's channel conditions, ER becomes an appropriate performance metric. Next, the ERs of S_u and S_f are calculated.

A. ER of S_u

When S_u accesses the channel, it holds that its ER can be expressed as [18]

$$\begin{aligned}\bar{C}_u&=\mathbb{E}\{\log_2(1+\gamma_{x_{u1}})\}+\mathbb{E}\{\log_2(1+\gamma_{x_{u2}})\}\\&\triangleq\bar{C}_{x_{u1}}+\bar{C}_{x_{u2}},\end{aligned}\tag{36}$$

where $\mathbb{E}\{\cdot\}$ denotes statistical expectation.

The following theorem returns S_u's ER.

Theorem 5. *Source's S_u ER under ipCSI can be calculated via*

$$\bar{C}_u=\bar{C}_{x_{u1}}+\bar{C}_{x_{u2}},\tag{37}$$

where $\bar{C}_{x_{u1}}$, $\bar{C}_{x_{u2}}$ are given by (38), (39), respectively, provided at the top of the next page, where $c=\frac{\hat{\lambda}_f\tilde{k}_2}{\hat{\lambda}_u}$ and $\text{Ei}(\cdot)$ denotes the exponential integral function [33, Eq. (8.211.1)].

Proof: The proof is provided in Appendix B. ■

Remark 6. *The ER of S_u under pCSI can be evaluated via (20) by setting $\sigma_{\epsilon_u}^2$, $\sigma_{\epsilon_f}^2$ equal to zero. On the other hand, similarly with other cases in the existing literature, $\bar{C}_u$ under pSIC cannot be given by just setting $\tilde{k}_1=\tilde{k}_2=0$ in (37).*

The following lemma provides the ER of S_u under pSIC.

Lemma 2. *The ER of S_u under pSIC can be given as*

$$\bar{C}_u^{p}=\bar{C}_{x_{u1}}-e^{\frac{D_1}{\hat{\lambda}_u a_2\rho}}\,\text{Ei}\left(-\frac{D_1}{\hat{\lambda}_u a_2\rho}\right).\tag{40}$$

Proof: The ER of S_u under pSIC can be given via (36) as soon as $\bar{C}_{x_{u2}}$ is properly updated in order to correspond to the pSIC case. In more detail, under pSIC, one obtains

$$\bar{C}_{x_{u2}}^{p}=\frac{1}{\ln 2}\int_0^{\infty}\frac{1-F_{\gamma_{x_{u2}}^{p}}(x)}{1+x}\mathrm{d}x,\tag{41}$$

where

$$\gamma_{x_{u2}}^{p}=\frac{a_2\rho|\hat{h}_u|^2}{D_1}.\tag{42}$$

By calculating the CDF of $\gamma_{x_{12}}^{p}$ as

$$\begin{aligned}F_{\gamma_{x_{u2}}^{p}}(x)&=F_{|\hat{h}_u|^2}\left(\frac{D_1x}{a_2\rho}\right)\\&=1-e^{-\frac{D_1x}{\hat{\lambda}_u a_2\rho}},\end{aligned}\tag{43}$$

then applying (43) into (41) and finally leveraging [33, Eq. (3.352.4)], (40) is deduced. ■

B. ER of x_f

In terms of S_f, taking into account (2), it holds that its ER can be given as

$$\begin{aligned}\bar{C}_f&=(1-q)\,\mathbb{E}\{\log_2(1+\gamma_{x_f}^{\text{OMA}})\}\\&\quad+\sum_{u\in\mathcal{U}}p_u\prod_{\substack{n\in\mathcal{U},\\ n\neq u}}(1-p_n)\,\mathbb{E}\{\log_2(1+\gamma_{x_f,u})\}\\&\triangleq(1-q)\,\bar{C}_{x_f}^{\text{OMA}}+\sum_{m\in\mathcal{U}}p_u\,\bar{C}_{x_f,u}^{\text{RSMA}}\prod_{\substack{n\in\mathcal{U},\\ n\neq u}}(1-p_n).\end{aligned}\tag{44}$$

The following theorem returns S_f's ER under ipCSI and ipSIC.

$$\bar{C}_{x_{u1}}=\begin{cases}-\frac{a_2}{a_1\ln 2}e^{\frac{D_1}{a_2\hat{\lambda}_u\rho}}\mathrm{Ei}\left(-\frac{D_1}{a_2\hat{\lambda}_u\rho}\right)+\frac{a_2}{a_1\ln 2}e^{\frac{D_1}{\hat{\lambda}_u\rho}}\mathrm{Ei}\left(-\frac{D_1}{\hat{\lambda}_u\rho}\right)+\frac{a_1}{(1-a_2)\ln 2}\left(\frac{D_1}{\hat{\lambda}_u\rho}e^{\frac{D_1}{\hat{\lambda}_u\rho}}\mathrm{Ei}\left(-\frac{D_1}{\hat{\lambda}_u\rho}\right)+1\right), & \hat{\lambda}_f=\hat{\lambda}_u\\ \frac{1}{a_1\ln 2}e^{\frac{D_1}{a_2\hat{\lambda}_u\rho}}\mathrm{Ei}\left(-\frac{D_1}{a_2\hat{\lambda}_u\rho}\right)-\frac{1}{a_1\ln 2}e^{\frac{D_1}{\hat{\lambda}_u\rho}}\mathrm{Ei}\left(-\frac{D_1}{\hat{\lambda}_u\rho}\right)+\frac{a_1}{a_2(a_2-1)\ln 2}\left(\frac{D_1}{\hat{\lambda}_u\rho}e^{\frac{D_1}{a_2\hat{\lambda}_u\rho}}\mathrm{Ei}\left(-\frac{D_1}{a_2\hat{\lambda}_u\rho}\right)+a_2\right), & \hat{\lambda}_f=a_2\hat{\lambda}_u\\ -\frac{a_1\hat{\lambda}_u}{\ln 2}\left(\frac{1}{\hat{\lambda}_f\left(1-\frac{a_2\hat{\lambda}_u}{\hat{\lambda}_f}\right)\left(1-\frac{\hat{\lambda}_u}{\hat{\lambda}_f}\right)}e^{\frac{D_1}{\hat{\lambda}_f\rho}}\mathrm{Ei}\left(-\frac{D_1}{\hat{\lambda}_f\rho}\right)+\frac{1}{a_2\left(\hat{\lambda}_u-\frac{\hat{\lambda}_f}{a_2}\right)\left(1-\frac{1}{a_2}\right)}e^{\frac{D_1}{a_2\hat{\lambda}_u\rho}}\mathrm{Ei}\left(-\frac{D_1}{a_2\hat{\lambda}_u\rho}\right)\right.\\ \qquad\left.+\frac{1}{a_1(\hat{\lambda}_u-\hat{\lambda}_f)}e^{\frac{D_1}{\hat{\lambda}_u\rho}}\mathrm{Ei}\left(-\frac{D_1}{\hat{\lambda}_u\rho}\right)\right), & \text{otherwise}\end{cases} \tag{38}$$

$$\bar{C}_{x_{u2}}=\begin{cases}\frac{a_1a_2\tilde{k}_1}{(\tilde{k}_1a_1-c)^2\ln 2}\left(e^{\frac{D_1}{c\hat{\lambda}_u\rho}}\mathrm{Ei}\left(-\frac{D_1}{c\hat{\lambda}_u\rho}\right)-e^{\frac{D_1}{\tilde{k}_1a_1\hat{\lambda}_u\rho}}\mathrm{Ei}\left(-\frac{D_1}{\tilde{k}_1a_1\hat{\lambda}_u\rho}\right)\right)-\frac{a_2}{c(\tilde{k}_1a_1-c)\ln 2}\left(\frac{D_1}{\hat{\lambda}_u\rho}e^{\frac{D_1}{c\hat{\lambda}_u\rho}}\mathrm{Ei}\left(-\frac{D_1}{c\hat{\lambda}_u\rho}\right)+c\right), & \frac{\hat{\lambda}_f}{\hat{\lambda}_u}=\frac{\tilde{k}_1a_1+a_2}{\tilde{k}_2}\\ \frac{\tilde{k}_1a_1+a_2}{a_2\ln 2}\left(e^{\frac{D_1}{\tilde{k}_1a_1\hat{\lambda}_u\rho}}\mathrm{Ei}\left(-\frac{D_1}{\tilde{k}_1a_1\hat{\lambda}_u\rho}\right)-e^{\frac{D_1}{a\hat{\lambda}_u\rho}}\mathrm{Ei}\left(-\frac{D_1}{a\hat{\lambda}_u\rho}\right)\right)-\frac{1}{\tilde{k}_1a_1\ln 2}\left(\frac{D_1}{\hat{\lambda}_u\rho}e^{\frac{D_1}{\tilde{k}_1a_1\hat{\lambda}_u\rho}}\mathrm{Ei}\left(-\frac{D_1}{\tilde{k}_1a_1\hat{\lambda}_u\rho}\right)+\tilde{k}_1a_1\right), & \frac{\hat{\lambda}_f}{\hat{\lambda}_u}=\frac{\tilde{k}_1a_1}{\tilde{k}_2}\\ -\frac{a_2\hat{\lambda}_u}{\ln 2}\left(\frac{1}{\hat{\lambda}_f\tilde{k}_2\left(1-\frac{\tilde{k}_1a_1}{c}\right)\left(1-\frac{\tilde{k}_1a_1+a_2}{c}\right)}e^{\frac{D_1}{\hat{\lambda}_f\tilde{k}_2\rho}}\mathrm{Ei}\left(-\frac{D_1}{\hat{\lambda}_f\tilde{k}_2\rho}\right)+\frac{1}{\tilde{k}_1a_1\left(\hat{\lambda}_u-\frac{\hat{\lambda}_f\tilde{k}_2}{\tilde{k}_1a_1}\right)\left(1-\frac{\tilde{k}_1a_1+a_2}{\tilde{k}_1a_1}\right)}e^{\frac{D_1}{\hat{\lambda}_u\tilde{k}_1a_1\rho}}\right.\\ \qquad\left.\times\mathrm{Ei}\left(-\frac{D_1}{\hat{\lambda}_u\tilde{k}_1a_1\rho}\right)+\frac{1}{(\tilde{k}_1a_1+a_2)\left(\hat{\lambda}_u-\frac{\hat{\lambda}_f\tilde{k}_2}{\tilde{k}_1a_1}a_2\right)\left(1-\frac{\tilde{k}_1a_1}{\tilde{k}_1a_1+a_2}\right)}e^{\frac{D_1}{\hat{\lambda}_u\rho(\tilde{k}_1a_1+a_2)}}\mathrm{Ei}\left(-\frac{D_1}{\hat{\lambda}_u\rho(\tilde{k}_1a_1+a_2)}\right)\right), & \text{otherwise}\end{cases} \tag{39}$$

Theorem 6. *S_f's ER under ipCSI and ipSIC can be evaluated as*

$$\bar{C}_f=\sum_{m\in\mathcal{U}}p_u\,\bar{C}^{\mathrm{RSMA}}_{x_f,u}\prod_{\substack{n\in\mathcal{U},\\ n\neq u}}(1-p_n)-(1-q)\,e^{\frac{D_2}{\hat{\lambda}_f\rho}}\mathrm{Ei}\left(-\frac{D_2}{\hat{\lambda}_f\rho}\right), \tag{45}$$

where $\bar{C}^{\mathrm{RSMA}}_{x_f,u}$ is given by (46) at the top of the next page.

Proof: When it comes to the OMA case, then it holds

$$\begin{aligned}\bar{C}^{\mathrm{OMA}}_{x_f}&=\frac{1}{\ln 2}\int_0^\infty\frac{1-F_{\gamma^{\mathrm{OMA}}_{x_f}}(x)}{1+x}\mathrm{d}x\\&=\frac{1}{\ln 2}\int_0^\infty\frac{e^{-\frac{\left(\rho\sigma^2_{\epsilon_f}+1\right)x}{\hat{\lambda}_f\rho}}}{1+x}\mathrm{d}x.\\&=-e^{\frac{\rho\sigma^2_{\epsilon_f}+1}{\hat{\lambda}_f\rho}}\mathrm{Ei}\left(-\frac{\rho\sigma^2_{\epsilon_f}+1}{\hat{\lambda}_f\rho}\right).\end{aligned} \tag{47}$$

On the other hand, for the RSMA case, it holds

$$\bar{C}^{\mathrm{RSMA}}_{x_f,u}=\frac{1}{\ln 2}\int_0^\infty\frac{1-F_{\gamma_{x_f,u}}(x)}{1+x}\mathrm{d}x. \tag{48}$$

By taking into account (7), we can evaluate RV's γ_{x_f} CDF as follows

$$\begin{aligned}F_{\gamma_{x_f,u}}(x)&=\Pr\left(\frac{\rho|\hat{h}_f|^2}{a_2\rho|\hat{h}_u|^2+\tilde{k}_1a_1\rho|\hat{h}_u|^2+D_1}<x\right)\\&=\int_0^\infty F_{|\hat{h}_f|^2}\left((a_2+\tilde{k}_1a_1)|\hat{h}_u|^2x+\frac{D_1x}{\rho}\right)f_{|\hat{h}_u|^2}(y)\,\mathrm{d}y\\&=1-e^{-\frac{D_1x}{\hat{\lambda}_f\rho}}\frac{\hat{\lambda}_f}{(a_2+\tilde{k}_1a_1)\hat{\lambda}_ux+\hat{\lambda}_f}.\end{aligned} \tag{49}$$

Invoking (49) in (48), yields

$$\bar{C}^{\mathrm{RSMA}}_{x_f,u}=\frac{1}{\ln 2}\int_0^\infty\frac{\hat{\lambda}_f}{(1+x)((a_2+\tilde{k}_1a_1)\hat{\lambda}_ux+\hat{\lambda}_f)}e^{-\frac{D_1x}{\hat{\lambda}_f\rho}}\mathrm{d}x. \tag{50}$$

If $(a_2+\tilde{k}_1a_1)\hat{\lambda}_u\neq\hat{\lambda}_f$, (50) can be rewritten as

$$\begin{aligned}\bar{C}^{\mathrm{RSMA}}_{x_f,u}=\frac{\hat{\lambda}_f}{\ln 2}\left(\int_0^\infty\frac{e^{-\frac{D_1x}{\hat{\lambda}_f\rho}}}{(\hat{\lambda}_f-(a_2+\tilde{k}_1a_1)\hat{\lambda}_u)(1+x)}\mathrm{d}x\right.\\\left.+\int_0^\infty\frac{e^{-\frac{D_1x}{\hat{\lambda}_f\rho}}}{\left(1-\frac{\hat{\lambda}_f}{(a_2+\tilde{k}_1a_1)\hat{\lambda}_u}\right)((a_2+\tilde{k}_1a_1)\hat{\lambda}_ux+\hat{\lambda}_f)}\mathrm{d}x\right).\end{aligned} \tag{51}$$

On the other hand, if $(a_2+\tilde{k}_1a_1)\hat{\lambda}_u=\hat{\lambda}_f$, (50) can be rewritten as

$$\bar{C}^{\mathrm{RSMA}}_{x_f,u}=\frac{1}{\ln 2}\int_0^\infty\frac{1}{(1+x)^2}e^{-\frac{D_1x}{\hat{\lambda}_f\rho}}\mathrm{d}x. \tag{52}$$

Invoking [33, Eq. (3.352.4)] in (51), [33, Eq. (3.353.3)] in (52) and then combining the resultants (51) and (52), (46) is derived, which completes the proof. ■

$$\bar{C}^{\text{RSMA}}_{x_f,u}=\begin{cases}\frac{1}{\ln 2}\left(\frac{D_1}{\hat{\lambda}_f\rho}e^{\frac{D_1}{\hat{\lambda}_f\rho}}\text{Ei}\left(-\frac{D_1}{\hat{\lambda}_f\rho}\right)+1\right), & \frac{(a_2+\tilde{k}_1a_1)\hat{\lambda}_u}{\hat{\lambda}_f}=1\\ -\frac{1}{\ln 2}\left(\frac{1}{(\hat{\lambda}_f-(a_2+\tilde{k}_1a_1)\hat{\lambda}_u)}e^{\frac{D_1}{\hat{\lambda}_f\rho}}\text{Ei}\left(-\frac{D_1}{\hat{\lambda}_f\rho}\right)+\frac{1}{(a_2+\tilde{k}_1a_1)\hat{\lambda}_u-\hat{\lambda}_f}e^{\frac{D_1}{\hat{\lambda}_u\rho(a_2+\tilde{k}_1a_1)}}\text{Ei}\left(-\frac{D_1}{\hat{\lambda}_u\rho(a_2+\tilde{k}_1a_1)}\right)\right), & \text{otherwise}\end{cases} \tag{46}$$

Remark 7. *The ER of S_f under pSIC can be evaluated by (46) as soon as parameters $\tilde{k}_1$, $\tilde{k}_2$ are set equal to zero. Likewise, S_f's ER under pCSI can be evaluated via (46) by setting $\sigma^2_{\epsilon_u}$, $\sigma^2_{\epsilon_f}$ equal to zero.*

C. Ergodic Sum Rate

Utilizing the extracted ER expressions for S_f and S_u, the ESR of the proposed system under ipCSI and ipSIC can be derived as

$$\bar{C}_{\text{sum}}=(1-q)\,\bar{C}^{\text{OMA}}_{x_f}+\sum_{u\in\mathcal{U}}p_u\left(\bar{C}_u+\bar{C}^{\text{RSMA}}_{x_f,u}\right)\prod_{\substack{n\in\mathcal{U},\\ n\neq u}}(1-p_n). \tag{53}$$

It is noted that for the case of pCSI, (53) still holds as soon as parameters $\sigma^2_{\epsilon_u}$, $\sigma^2_{\epsilon_f}$ are set equal to zero, while for the case of pSIC, (53) still holds as soon as $\bar{C}_u$ is replaced with $\bar{C}^p_u$ and parameters $\tilde{k}_1$, $\tilde{k}_2$ are set equal to zero. It is further highlighted that by setting $\bar{C}^{\text{RSMA}}_{x_f,u}=0$, the second term of (53) returns the sum of umMTC sources' ERs.

D. High SNR regime

In this section, sources' ER asymptotic performance at high SNRs is investigated.

Lemma 3. *At the high SNR regime and under ipCSI and ipSIC, both S_u and S_f show ER floors that can be evaluated via (37), (45), respectively, by replacing D_j with $\tilde{D}_j=D_j-1$, where $j\in\{1,2\}$.*

Proof: The proof can be straightforwardly obtained by following the same procedure as in the proof of Lemma 1. ■

Remark 8. *From the above lemma, it becomes obvious that sources' ER floors are directly affected from the ipCSI and ipSIC parameters.*

Remark 9. *For the case of ipCSI and pSIC, the asymptotic expression for $\bar{C}_f$ provided in Lemma 3 still holds as soon as parameters $\tilde{k}_1$, $\tilde{k}_2$ are set equal to zero. On the other hand, for $\bar{C}_u$, an asymptotic expression can be obtained via (40) as soon as the approximation $D_1=\rho\sigma^2_{\epsilon_u}+\rho\sigma^2_{\epsilon_f}+1\to\rho\sigma^2_{\epsilon_u}+\rho\sigma^2_{\epsilon_f}$ when $\rho\to\infty$ is used. Furthermore, for the case of pCSI (and pSIC or ipSIC), the arguments of both exponential functions and exponential integral functions in (40), (38) and (46) have the form of $\frac{G}{B\rho}$. Hence, by applying the approximations $e^{x\to 0}(-x)=1-x$ and $\text{Ei}^{x\to 0}(x)=C+\ln(-x)$, where C is the Euler constant, then asymptotic expressions can be obtained.*

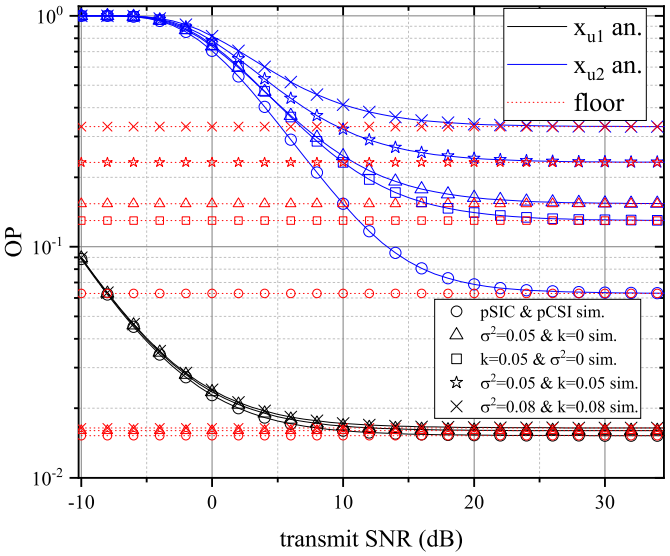

Fig. 1: OPs of messages x_{u1}, x_{u2} vs ρ for different σ^2, k values.

V. Numerical Results and Discussion

In this section, analytical (an.) and simulation (sim.) results are presented to verify the presented analysis as well as to investigate how the different system parameters affect the performance of the presented system model. For the extraction of the following figures, unless otherwise stated, $a_1=0.9$, $\beta_u=0.1$, $\hat{\lambda}_u=1$, $\hat{\lambda}_f=2$, $R_u=0.1$ bps/Hz with $u\in\mathcal{U}$, $R_f=1$ bps/Hz, $N=10$, $p_u=p=0.2$, and thus $q=0.2684$ are assumed. Furthermore, for convenience, it is assumed that $\tilde{k}_1=\tilde{k}_2=k$ and $\sigma^2_{\epsilon_u}=\sigma^2_{\epsilon_f}=\sigma^2$.

In Fig. 1, the OPs of messages x_{u1}, x_{u2} with respect to transmit SNR ρ are provided for different values of σ^2 and k. It can be observed that simulations results coincide with the analytical ones, thus, verifying the presented analysis. Furthermore, it is obvious that both messages reach outage floors at the high SNR regime which also appear to depend on the values of k and σ^2. This observation further validates Remark 5. Focusing on x_{u2}, under pCSI and ipSIC with $k=0.05$, the OP of x_{u2} achieves equal or lower values compared to the case of pSIC and ipCSI with $\sigma^2=0.05$. This observation provides the insight that ipCSI has a more detrimental effect on the OP of x_{u2} compared to SIC propagation error and can be explained by the fact that ipCSI affects all the SINR terms that appear in (19), while ipSIC affects only two of them. On the other hand, regarding x_{u1}, it is obvious that ipSIC does not affect its OP, since this message is decoded first at the BS side. These insights clearly indicate the importance of careful RS parameter β_u selection since each

This article has been accepted for publication in IEEE Transactions on Communications. This is the author's version which has not been fully edited and content may change prior to final publication. Citation information: DOI 10.1109/TCOMM.2024.3403502

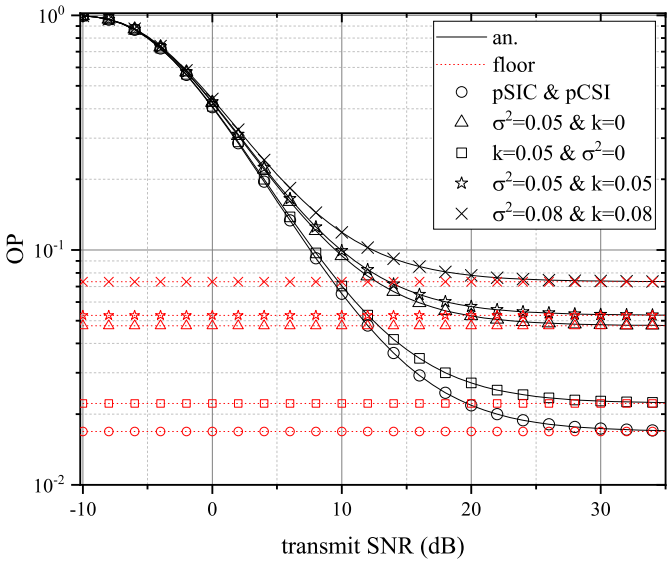

Fig. 2: OP of message x_f vs ρ for different σ^2, k values.

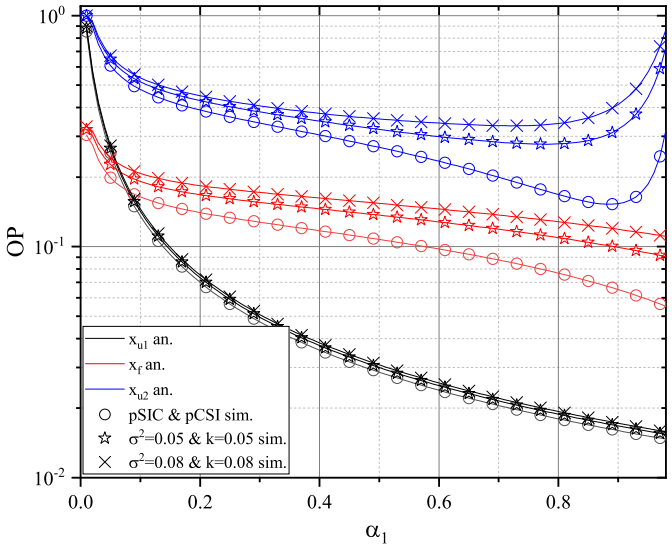

Fig. 3: OPs of messages x_{u1}, x_f, x_{u2} vs power allocation a_1 for different σ^2, k values when $\rho=10$ dB.

of S_u's substreams is uniquely affected from ipCSI and ipSIC. Furthermore, regarding x_{u1}, it is illustrated that its outage behavior remains relatively robust against ipSIC and ipCSI, since its outage performance when $k = \sigma^2 = 0.08$ remains really close to the achieved performance performance when $k = \sigma^2 = 0.05$.

In Fig. 2, the OP of message x_f versus transmit SNR ρ for different ipSIC and ipCSI parameters is depicted. Similarly with the cases of x_{u1} and x_{u2}, x_f achieves outage floors at high SNR values. Also, likewise the case of x_{u2}, the impact of ipCSI seems to be more severe for S_f's outage performance compared to ipSIC. This can be explained by considering the fact that with probability $(1-q) \approx 0.73$, S_f accesses the wireless medium solely, i.e., in an orthogonal manner and, thus, ipSIC does not affect the performance of x_f for 73% of the cases. On the other hand, as (4) witnesses, even when S_f accesses the channel in a solely manner, ipCSI affects the outage behavior of x_f. Furthermore, as expected, as both k and σ^2 increase, the OP of x_f also increases. This can be seen by comparing the performance of x_f when $k = \sigma^2 = 0.05$ versus when $k = \sigma^2 = 0.08$.

In Fig. 3, the OPs of messages x_{u1}, x_f, x_{u2} as a function of power allocation a_1 are illustrated. It can be observed that, for all cases, as a_1 increases, the OPs of both x_{u1} and x_f decrease. On the other hand, x_{u2}'s OP shows a convex behavior, i.e., as a_1 increases, the OP of x_{u2} decreases up to a specific value and then begins to increase. To explain this convex behavior we should recall that, as it is also evident by (19), for the successful decoding of x_{u2} both inequalities $\gamma_{x_{u1}} > r_{u1}$ and $\gamma_{x_f,u} > r_f$ must hold. As previously noted, the increase of a_1 leads to increase of $\gamma_{x_{u1}}$ and γ_{x_f}, however, as (8) witnesses, it also leads to decrease of $\gamma_{x_{u2}}$. Hence, the increase of a_1 leads to an increased probability that $\gamma_{x_{u1}} > r_{u1}$ and $\gamma_{x_f,u} > r_f$ hold and, thus, the probability of (19) increases as soon as the probability that the inequality $\gamma_{x_{u2}} > r_{u2}$ holds remains relatively large. However, there exists an a_1 threshold after which further increase of a_1 begins to considerably decrease

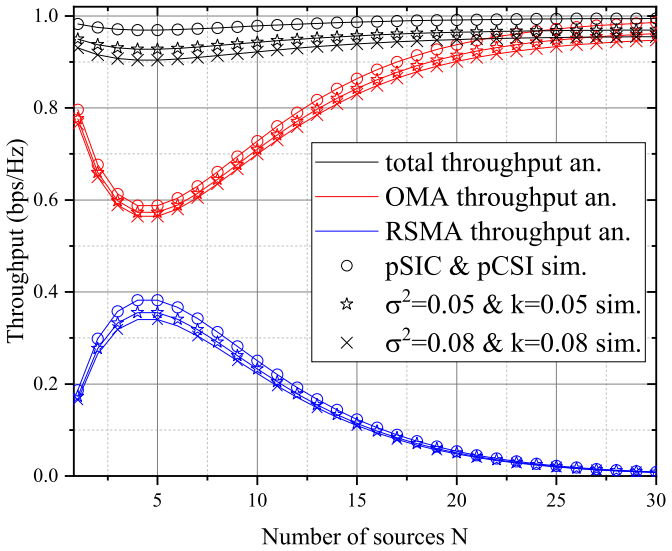

Fig. 4: FeMBB source's throughput vs N for different σ^2, k values.

the probability that the inequality $\gamma_{x_{u2}} > r_{u2}$ holds, thus increasing the OP of x_{u2}. From all the above, it occurs that after a specific value, the further increase of a_1 raises a trade-off regarding feMBB and umMTC services performance since increased a_1 leads to decreased S_f's OP but increased OP of S_u's substream x_{u2}.

In Fig. 4, the throughput of S_f with respect to the number of umMTC sources N assigned to share the same resource blocks with S_f is shown for different values of k and σ^2 when $\rho=20$ dB. As OMA throughput we refer to the throughput achieved when S_f transmits without interference from the umMTC sources, i.e., the first term of (32), while as RSMA throughput we refer to the throughput achieved when S_f transmits non-orthogonally alongside a umMTC source, i.e., the second term of (32). The total throughput is the sum of the two cases above.

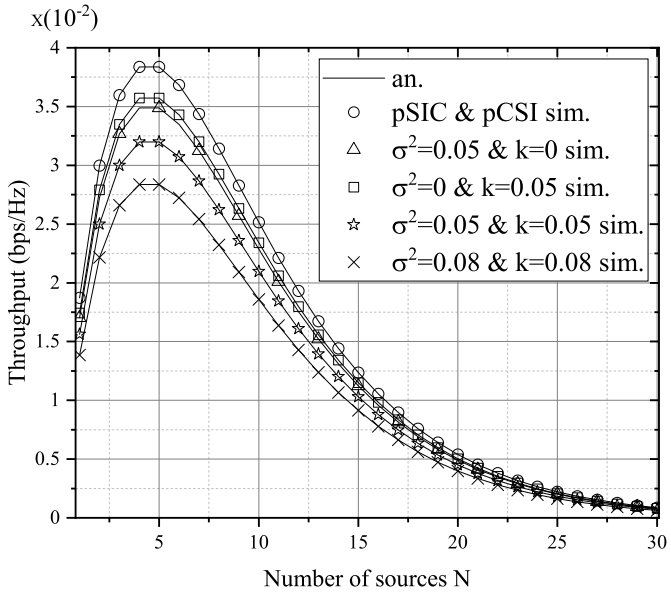

Fig. 5: UmMTC sources' sum throughput vs N for different σ^2, k values.

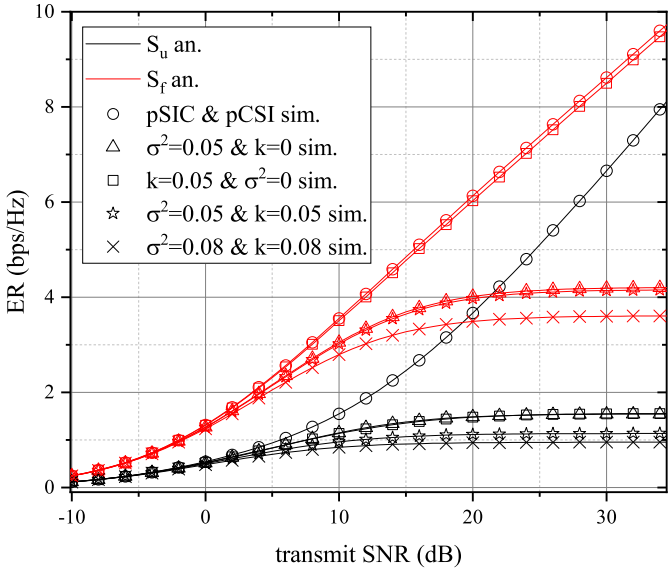

Fig. 6: Sources' ERs vs ρ for different σ^2, k and q values.

It occurs that both OMA and RSMA throughput show a convex behavior, with the latter reaching its highest value when the former reaches its lowest value, i.e., when $N = 5$. This happens because for fixed $p = 0.2$, $N = 5$ gives the highest probability that only one of the umMTC sources accesses the channel, and thus RSMA is used more frequently compared to other N values. Specifically, (2) shows that for $p = 0.2$ and $N = 5$, RSMA is used for 40.96% of the transmissions. Interestingly, it is also shown that for fixed σ^2, k values, the total throughput of S_f remains relatively constant over $N \in [1, 30]$ values. This is an important observation, since it implies that the proposed access scheme allows the throughput performance of the feMBB source to remain robust to an increased number of umMTC sources assigned to transmit in the initially allocated resource blocks of S_f.

In Fig. 5, the sum throughput of umMTC sources is plotted with respect to their total number N for different k and σ^2 values when $\rho = 20$ dB. Similar to the OMA and RSMA curves shown in Fig. 4, it can be seen that the total throughput of the umMTC sources also behaves in a convex manner, with its highest value being reached when $N = 5$. This was expected since, as explained earlier, the probability of one of the umMTC sources accessing the wireless medium is highest for $N = 5$. For values $N > 5$, the total number of collisions between the umMTC sources gradually increases, resulting in no umMTC transmissions and thus lower overall throughput gains. On the other hand, for $N < 5$ values, the sparse activity of the umMTC sources, i.e., each of them accesses the channel with probability $p = 0.2$, leads to an increased number of unoccupied slots, which negatively affects the total throughput of the umMTC sources. In summary, the total number of umMTC sources and their sporadic activity are two factors that need to be seriously considered when designing heterogeneous networks.

In Fig. 6, S_f's and S_u's ERs are illustrated in terms of transmit SNR for different k and σ^2 values. First of all, it can be highlighted that S_u achieves floors at the high SNR regime when ipSIC or ipCSI is applied. On the other hand, S_f appears to avoid floor values at the high SNRs when pCSI is applied even if ipSIC is considered, since, with probability $(1 - q) = 73.16\%$, S_f accesses the channel in an orthogonal manner and when OMA with pCSI is applied then no ER floors appear. For the same reason, i.e., because S_f frequently accesses the channel via OMA and, thus, is only affected by ipCSI, its ER performance when $\sigma^2 = 0$ and $k = 0.05$ is better than when $\sigma^2 = 0.05$ and $k = 0$. In fact, for the ipSIC, pCSI case, feMBB source's ER performance is pretty close to the pSIC, pCSI case. On the other hand, when it comes to the umMTC source, ipCSI and ipSIC have a similar impact on its ER. This can be concluded by observing that its ER performance when $\sigma^2 = 0$ and $k = 0.05$ and when $\sigma^2 = 0.05$ and $k = 0$. Finally, as Remark 8 highlights, the floors obtained by both sources at the high SNR regime depend on the ipSIC and ipCSI parameters, thus the importance of the inclusion of such imperfections in the investigation of such systems is demonstrated. From all of the above, it appears that the presented hybrid OMA-RSMA access scheme provides the ability to control the level of ipSIC that affects the ER performance of feMBB sources, and thus remains robust to the practical limitations of ipSIC that arise in real-world applications. This is important when considering their high data rate requirements.

In Fig. 7, the ER of S_f, umMTC sources sum ERs, which can be easily derived from (53), and the total ESR of the system are plotted together with the number of umMTC sources, N. As expected, with increasing values of σ^2 and k, both the ER of S_f and the sum of the ERs of the umMTC sources decrease. Furthermore, similar to Fig. 4, for fixed values of σ^2, k, the ER of S_f achieves its lowest value when the sum of the ERs of the umMTC sources reaches its highest value. As already explained, this is due to the frequent time slot sharing between S_f and umMTC sources when $p = 0.2$ and $N = 5$. Meanwhile, interestingly, for fixed

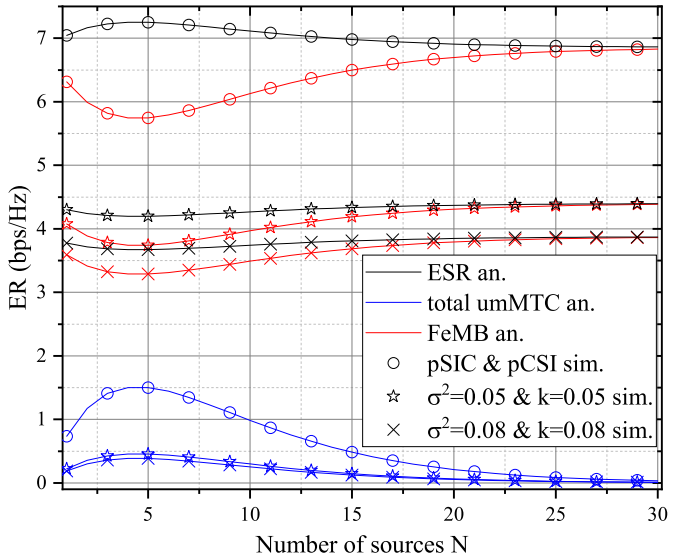

Fig. 7: feMBB source's ER, umMTC sources' total ER and system's ESR vs N for different σ^2, k and q values.

values of σ^2 and k, the system's ESR seems to remain robust to the increased number of umMTC sources. Specifically, under pCSI, pSIC, despite the increased interference levels due to the frequent use of RSMA when $N = 5$, the system's total ESR reaches its highest value. This is due to the collision mechanism adopted regarding access to umMTC sources. This implies that the careful design of the access scheme in a hybrid orthogonal and non-orthogonal manner allows not only to serve the large number of umMTC sources in 6G networks, but also to increase the overall system performance.

VI. Conclusion

In this work, we considered a communication scenario assuming the coexistence of multiple feMBB as well as umMTC sources in a wireless network. feMBB sources were assumed to have always information to transmit to the BS, while umMTC sources were assumed to probabilistically access each specific slot. Towards enhanced connectivity, feMBB and umMTC services are allowed to share the same resources. In this context, when feMBB and umMTC sources simultaneously access the network, uplink RSMA was utilized for their transmissions. For the presented setup, novel closed-form expressions were derived for sources' OP and ERs as well as the overall outage throughput and ESR under all pSIC, ipSIC, pCSI, ipCSI cases. Moreover, the asymptotic outage as well as ER behavior of sources was investigated at high SNRs and useful insights regarding the appearance of OP and ER floors were provided. Simulation results revealed the authenticity of the presented analysis, illustrated how different system parameters affect sources' and system's performance, and revealed the detrimental impact of CSI and SIC imperfections compared to the ideal case of pCSI and pSIC. As a future direction, the performance of the proposed hybrid access scheme in the context of multi-antenna BS configurations can be examined.

Appendix A
Proof of Theorem 2

Taking into account (2), (13) and (14), yields

$$P_{f,u}^{o} = (1-q)P_f^{\text{OMA}} + \sum_{u\in\mathcal{U}} p_u\, P_{f,u}^{\text{RSMA}} \prod_{\substack{n\in\mathcal{U},\\ n\neq u}} (1-p_n). \quad (54)$$

For the OMA case, invoking (4) in (13), it occurs

$$P_f^{\text{OMA}} = 1 - e^{-\frac{\rho\sigma_{\epsilon_f}^2 r_f + r_f}{\lambda_f \rho}}. \quad (55)$$

On the other hand, when RSMA is applied, by invoking (6), (7) in (14), one obtains

$$P_{f,u}^{\text{RSMA}} = 1 - \Pr\left(\frac{a_1\rho|\hat{h}_u|^2}{\rho|\hat{h}_f|^2 + a_2\rho|\hat{h}_u|^2 + D_1} > r_{u1}, \frac{\rho|\hat{h}_f|^2}{a_2\rho|\hat{h}_u|^2 + \tilde{k}_1 a_1\rho|\hat{h}_u|^2 + D_1} > r_f\right). \quad (56)$$

After some algebraic manipulations, (56) can be transformed into

$$P_{f,u}^{\text{RSMA}} = \begin{cases} 1 - P_{f,u}^{\text{A}}, & \frac{a_1}{a_2} > r_{u1} \\ 1, & \text{otherwise,} \end{cases} \quad (57)$$

where

$$P_{f,u}^{\text{A}} = 1 - \Pr\left(|\hat{h}_u|^2 > \frac{\rho|\hat{h}_f|^2 r_{u1} + D_1 r_{u1}}{a_1\rho - a_2\rho r_{u1}}, |\hat{h}_u|^2 < \frac{\rho|\hat{h}_f|^2 - D_1 r_f}{a_2\rho r_f + \tilde{k}_1 a_1\rho r_f}\right). \quad (58)$$

In what follows, we focus on the evaluation of $P_{f,u}^{\text{A}}$. In order that $P_{f,u}^{\text{A}}$ takes non-zero values, it must hold

$$\frac{\rho|\hat{h}_f|^2 r_{u1} + D_1 r_{u1}}{a_1\rho - a_2\rho r_{u1}} < \frac{\rho|\hat{h}_f|^2 - D_1 r_f}{a_2\rho r_f + \tilde{k}_1 a_1\rho r_f}. \quad (59)$$

After some manipulations, (59) becomes

$$|\hat{h}_f|^2 \left(\frac{\rho r_{u1}}{a_1\rho - a_2\rho r_{u1}} - \frac{\rho}{a_2\rho r_f + \tilde{k}_1 a_1\rho r_f}\right) < - \frac{D_1 r_f}{a_2\rho r_f + \tilde{k}_1 a_1\rho r_f} - \frac{D_1 r_{u1}}{a_1\rho - a_2\rho r_{u1}}. \quad (60)$$

In order for (60) to be valid, the following inequality must hold

$$\frac{\rho r_{u1}}{a_1\rho - a_2\rho r_{u1}} - \frac{\rho}{a_2\rho r_f + \tilde{k}_1 a_1\rho r_f} < 0. \quad (61)$$

If (61) holds, then (60) becomes

$$|\hat{h}_f|^2 > \frac{-\frac{D_1 r_f}{a_2\rho r_f + \tilde{k}_1 a_1\rho r_f} - \frac{D_1 r_{u1}}{a_1\rho - a_2\rho r_{u1}}}{\frac{\rho r_{u1}}{a_1\rho - a_2\rho r_{u1}} - \frac{\rho}{a_2\rho r_f + \tilde{k}_1 a_1\rho r_f}} = A, \quad (62)$$

where A is given in (18). Considering all the above, $P_{f,u}^{\text{A}}$ can be finally calculated as

$$P_{f,u}^{\text{A}} = \Pr\left(\frac{\rho|\hat{h}_f|^2 r_{u1} + D_1 r_{u1}}{a_1\rho - a_2\rho r_{u1}} < |\hat{h}_u|^2 < \frac{\rho|\hat{h}_f|^2 - D_1 r_f}{a_2\rho r_f + \tilde{k}_1 a_1\rho r_f}, |\hat{h}_f|^2 > A\right). \quad (63)$$

Leveraging RV's $|\hat{h}_f|^2$ PDF as well as RV's $|\hat{h}_u|^2$ CDF, it occurs

$$P_{f,u}^{\mathrm{A}} = \underbrace{\int_A^\infty F_{|\hat{h}_u|^2}\left(\frac{\rho y - D_1 r_f}{a_2\rho r_f + \tilde{k}_1 a_1 \rho r_f}\right) f_{|\hat{h}_f|^2}(y)\mathrm{d}y}_{I_1} - \underbrace{\int_A^\infty F_{|\hat{h}_u|^2}\left(\frac{\rho r_{u1} y + D_1 r_{u1}}{a_1\rho - a_2\rho r_{u1}}\right) f_{|\hat{h}_f|^2}(y)\mathrm{d}y}_{I_2}. \tag{64}$$

In terms of I_1, substituting $F_{|\hat{h}_u|^2}$ and $f_{|\hat{h}_f|^2}$, it occurs

$$\begin{aligned} I_1 &= 1 - \frac{1}{\hat{\lambda}_f} e^{\frac{D_1 r_f}{\hat{\lambda}_u(a_2\rho r_f + \tilde{k}_1 a_1 \rho r_f)}} \int_A^\infty e^{-y\left(\frac{1}{\hat{\lambda}_f} + \frac{1}{\hat{\lambda}_u(a_2 r_f + \tilde{k}_1 a_1 r_f)}\right)} \\ &= 1 - \frac{1}{1 + \frac{\hat{\lambda}_f}{\hat{\lambda}_u(a_2 r_f + \tilde{k}_1 a_1 r_f)}} e^{\frac{D_1 r_f - A\rho}{\hat{\lambda}_u(a_2\rho r_f + \tilde{k}_1 a_1 \rho r_f)} - \frac{A}{\hat{\lambda}_f}}. \end{aligned} \tag{65}$$

Following similar lines with I_1, I_2 can be extracted as follows

$$I_2 = 1 - \frac{1}{1 + \frac{\hat{\lambda}_f \rho r_{u1}}{\hat{\lambda}_u(a_1\rho - a_2\rho r_{u1})}} e^{-\frac{D_1 r_{u1} + \rho r_{u1} A}{\hat{\lambda}_u(a_1\rho - a_2\rho r_{u1})} - \frac{A}{\hat{\lambda}_f}}. \tag{66}$$

Invoking (65) and (66) in (64), while taking into account the condition of (61), (16) occurs. By finally applying (55) and (16) in (54), (15) is deduced which concludes the proof.

Appendix B
Proof of Theorem 5

In terms of $\bar{C}_{x_{u1}}$, it holds

$$\begin{aligned} \bar{C}_{x_{u1}} &= \int_0^\infty \log_2(1+\gamma) f_{\gamma_{x_{u1}}}(\gamma)\mathrm{d}\gamma \\ &\overset{(\alpha)}{=} \frac{1}{\ln 2}\int_0^{\frac{a_1}{a_2}} \frac{1 - F_{\gamma_{x_{11}}}(x)}{1+x}\mathrm{d}x, \end{aligned} \tag{67}$$

where step (α) occurs by leveraging [34, Eq. (28)]. By taking into account the definition of $F_{\gamma_{x_{u1}}}$, i.e., $F_{\gamma_{x_{u1}}}(x) = \Pr(\gamma_{x_{u1}} < x)$, it becomes obvious that the CDF of $\gamma_{x_{11}}$ can be given by (10) as soon as r_{u1} is replaced by x. Hence, (67) becomes

$$\bar{C}_{x_{u1}} = \frac{1}{\hat{\lambda}_f \ln 2}\int_0^{\frac{a_1}{a_2}} \frac{e^{-\frac{D_1 x}{\hat{\lambda}_u\rho(a_1 - a_2 x)}}}{(1+x)(\frac{x}{\hat{\lambda}_u(a_1 - a_2 x)} + \frac{1}{\hat{\lambda}_f})}\mathrm{d}x. \tag{68}$$

Unfortunately, the above integral cannot be calculated in closed-form in its current form. By changing variable of $y = \frac{x}{a_1 - a_2 x}$ in (68) and after some algebraic manipulations, it occurs

$$\bar{C}_{x_{u1}} = \frac{a_1\hat{\lambda}_u}{\ln 2}\int_0^\infty \frac{1}{(\hat{\lambda}_u + \hat{\lambda}_f y)(1+a_2 y)(1+y)} e^{-\frac{D_1 y}{\hat{\lambda}_u \rho}}\mathrm{d}y. \tag{69}$$

At this point, we must perform an extensive investigation regarding the exact form of the denumerator that appears in (69). If $\frac{\hat{\lambda}_f}{\hat{\lambda}_u} \neq a_2 \neq 1$, applying partial fraction decomposition in (69), we get

$$\begin{aligned} \bar{C}_{x_{u1}} = \frac{a_1\hat{\lambda}_u}{\ln 2}\Bigg(&\int_0^\infty \frac{1}{(1 - \frac{a_2\hat{\lambda}_u}{\hat{\lambda}_f})(1 - \frac{\hat{\lambda}_u}{\hat{\lambda}_f})} \frac{e^{-\frac{D_1 y}{\hat{\lambda}_u\rho}}}{\hat{\lambda}_u + \hat{\lambda}_f y}\mathrm{d}y \\ &+ \int_0^\infty \frac{1}{(\hat{\lambda}_u - \frac{\hat{\lambda}_f}{a_2})(1 - \frac{1}{a_2})} \frac{e^{-\frac{D_1 y}{\hat{\lambda}_u\rho}}}{1 + a_2 y}\mathrm{d}y \\ &+ \int_0^\infty \frac{1}{a_1(\hat{\lambda}_u - \hat{\lambda}_f)} \frac{e^{-\frac{D_1 y}{\hat{\lambda}_u\rho}}}{1+y}\mathrm{d}y\Bigg). \end{aligned} \tag{70}$$

Invoking [33, Eq. (3.352.4)] in (70) we get the third branch of (38) given at the top of page 9.

On the other hand, if $\frac{\hat{\lambda}_f}{\hat{\lambda}_u} = 1$, then (69) becomes

$$\bar{C}_{x_{u1}} = \frac{a_1}{\ln 2}\int_0^\infty \frac{1}{(1+a_2 y)(1+y)^2} e^{-\frac{D_1 y}{\hat{\lambda}_u\rho}}\mathrm{d}y. \tag{71}$$

Applying partial fraction decomposition in (71), it occurs

$$\begin{aligned} \bar{C}_{x_{u1}} = \frac{a_1}{\ln 2}\Bigg(&\int_0^\infty \frac{a_2^2}{a_1^2(1+a_2 y)} e^{-\frac{D_1 y}{\hat{\lambda}_u\rho}}\mathrm{d}y \\ &- \int_0^\infty \frac{a_2}{a_1^2(1+y)} e^{-\frac{D_1 y}{\hat{\lambda}_u\rho}}\mathrm{d}y \\ &+ \int_0^\infty \frac{1}{(1-a_2)(1+y)^2} e^{-\frac{D_1 y}{\hat{\lambda}_u\rho}}\mathrm{d}y\Bigg). \end{aligned} \tag{72}$$

By applying [33, Eq. (3.352.4)] and [33, Eq. (3.353.3)], we get the first branch of (38).

Finally, if $\frac{\hat{\lambda}_f}{\hat{\lambda}_u} = a_2 \neq 1$, then (69) becomes

$$\bar{C}_{x_{u1}} = \frac{a_1}{\ln 2}\int_0^\infty \frac{1}{(1+a_2 y)^2(1+y)} e^{-\frac{D_1 y}{\hat{\lambda}_u\rho}}\mathrm{d}y. \tag{73}$$

Evaluating (73) in a similar manner with (71), the second branch of (38) occurs.

In terms of $\bar{C}_{x_{u2}}$, it holds

$$\bar{C}_{x_{u2}} = \frac{1}{\ln 2}\int_0^\infty \frac{1 - F_{\gamma_{x_{u2}}}(x)}{1+x}\mathrm{d}x. \tag{74}$$

Hence, as a first step, we must calculate RV's $\gamma_{x_{12}}$ CDF, as follows

$$\begin{aligned} F_{\gamma_{x_{u2}}}(x) &= \Pr(\gamma_{x_{u2}} < x) \\ &= \Pr\left(\frac{a_2\rho|\hat{h}_u|^2}{\tilde{k}_1 a_1\rho|\hat{h}_u|^2 + \tilde{k}_2\rho|\hat{h}_f|^2 + D_1} < x\right) \\ &= \begin{cases} \int_0^\infty F_{|\hat{h}_u|^2}\left(\frac{\tilde{k}_2\rho y x + D_1 x}{a_2\rho - \tilde{k}_1 a_1\rho x}\right) f_{|\hat{h}_f|^2}(y)\,\mathrm{d}y, & x < \frac{a_2}{\tilde{k}_1 a_1} \\ 1, & \text{otherwise.} \end{cases} \end{aligned} \tag{75}$$

Substituting $F_{|\hat{h}_u|^2}$, $f_{|\hat{h}_f|^2}$ and performing some algebraic manipulations, it occurs

$$F_{\gamma_{x_{u2}}}(x) = \begin{cases} 1 - \frac{1}{1 + \frac{\hat{\lambda}_f\tilde{k}_2 x}{\hat{\lambda}_u(a_2 - \tilde{k}_1 a_1 x)}} e^{-\frac{D_1 x}{\hat{\lambda}_u\rho(a_2 - \tilde{k}_1 a_1 x)}}, & x < \frac{a_2}{\tilde{k}_1 a_1} \\ 1, & \text{otherwise.} \end{cases} \tag{76}$$

Invoking (76) in (74), we get

$$\bar{C}_{x_{u2}} = \frac{1}{\ln 2}\int_0^{\frac{a_2}{\tilde{k}_1 a_1}} \frac{e^{-\frac{D_1 x}{\hat{\lambda}_u \rho(a_2-\tilde{k}_1 a_1 x)}}}{(1+x)(1+\frac{\hat{\lambda}_f \tilde{k}_2 x}{\hat{\lambda}_u(a_2-\tilde{k}_1 a_1 x)})}\mathrm{d}x. \quad (77)$$

Changing variable of $y = \frac{x}{a_2-\tilde{k}_1 a_1 x}$ in (77), it follows that

$$\bar{C}_{x_{u2}} = \int_0^{\infty} \frac{a_2 \hat{\lambda}_u e^{-\frac{D_1 y}{\hat{\lambda}_u \rho}}}{(\hat{\lambda}_u + \hat{\lambda}_f \tilde{k}_2 y)(1+\tilde{k}_1 a_1 y)(1+(\tilde{k}_1 a_1 + a_2)y)}\mathrm{d}y. \quad (78)$$

It becomes apparent that (78) has a similar form with (69). Hence, for the evaluation of (78), we must take into consideration three different cases, namely

- $\frac{\hat{\lambda}_f \tilde{k}_2}{\hat{\lambda}_u} \neq \tilde{k}_1 a_1 \neq (\tilde{k}_1 a_1 + a_2)$
- $\frac{\hat{\lambda}_f k_2}{\hat{\lambda}_u} = \tilde{k}_1 a_1 \neq (\tilde{k}_1 a_1 + a_2)$
- $\frac{\hat{\lambda}_f k_2}{\hat{\lambda}_u} = (\tilde{k}_1 a_1 + a_2) \neq \tilde{k}_1 a_1$

and perform partial fraction decomposition for each case. It is noted that the above explained calculations can be performed in a similar manner with those performed for the evaluation of (69), and thus are omitted. By executing the above explained procedure, (39) given at the top of page 9 can be obtained, which completes the proof.

REFERENCES

[1] K. David and H. Berndt, "6G vision and requirements: Is there any need for beyond 5G?" *IEEE Veh. Technol. Mag.*, vol. 13, no. 3, pp. 72–80, Sep. 2018.

[2] Z. Zhang, Y. Xiao, Z. Ma, M. Xiao, Z. Ding, X. Lei, G. K. Karagiannidis, and P. Fan, "6G wireless networks: Vision, requirements, architecture, and key technologies," *IEEE Veh. Technol. Mag.*, vol. 14, no. 3, pp. 28–41, Sep. 2019.

[3] W. Saad, M. Bennis, and M. Chen, "A vision of 6G wireless systems: Applications, trends, technologies, and open research problems," *IEEE Netw.*, vol. 34, no. 3, pp. 134–142, May 2019.

[4] Y. Liu, S. Zhang, X. Mu, Z. Ding, R. Schober, N. Al-Dhahir, E. Hossain, and X. Shen, "Evolution of NOMA toward next generation multiple access (NGMA) for 6G," *IEEE J. Sel. Areas Commun.*, vol. 40, no. 4, pp. 1037–1071, Apr. 2022.

[5] P. D. Diamantoulakis, N. D. Chatzidiamantis, A. L. Moustakas, and G. K. Karagiannidis, "Next generation multiple access: Performance gains from uplink MIMO-NOMA," *IEEE Open J. Commun. Soc.*, vol. 3, pp. 2298–2313, Nov. 2022.

[6] B. Clerckx, Y. Mao, E. A. Jorswieck, J. Yuan, D. J. Love, E. Erkip, and D. Niyato, "A primer on rate-splitting multiple access: Tutorial, myths, and frequently asked questions," *IEEE J. Sel. Areas Commun.*, May 2023.

[7] Y. Mao, O. Dizdar, B. Clerckx, R. Schober, P. Popovski, and H. V. Poor, "Rate-splitting multiple access: Fundamentals, survey, and future research trends," *IEEE Commun. Surveys Tuts.*, 4th Quart. 2022.

[8] O. Dizdar, Y. Mao, W. Han, and B. Clerckx, "Rate-splitting multiple access: A new frontier for the PHY layer of 6G," in *Proc. IEEE 92nd Veh. Technol. Conf. (VTC-Fall)*. IEEE, Nov. 2020, pp. 1–7.

[9] A. Mishra, Y. Mao, O. Dizdar, and B. Clerckx, "Rate-splitting multiple access for 6G—part I: Principles, applications and future works," *IEEE Commun. Lett*, vol. 26, no. 10, pp. 2232–2236, Oct. 2022.

[10] B. Rimoldi and R. Urbanke, "A rate-splitting approach to the Gaussian multiple-access channel," *IEEE Trans. Inf. Theory*, vol. 42, no. 2, pp. 364–375, Mar. 1996.

[11] Y. Zhu, X. Wang, Z. Zhang, X. Chen, and Y. Chen, "A rate-splitting non-orthogonal multiple access scheme for uplink transmission," in *Proc. 9th Int. Conf. Wireless Commun. Signal Process. (WCSP), Nanjing, China*, Oct. 2017, pp. 1–6.

[12] H. Liu, T. A. Tsiftsis, K. J. Kim, K. S. Kwak, and H. V. Poor, "Rate splitting for uplink NOMA with enhanced fairness and outage performance," *IEEE Trans. Wireless Commun.*, vol. 19, no. 7, pp. 4657–4670, Jul. 2020.

[13] S. A. Tegos, P. D. Diamantoulakis, and G. K. Karagiannidis, "On the performance of uplink rate-splitting multiple access," *IEEE Commun. Lett.*, vol. 26, no. 3, pp. 523–527, Mar. 2022.

[14] H. Lu, X. Xie, Z. Shi, H. Lei, N. Zhao, and J. Cai, "Outage performance of uplink rate splitting multiple access with randomly deployed users," *IEEE Trans. Wireless Commun.*, Jun. 2023.

[15] O. Abbasi and H. Yanikomeroglu, "Transmission scheme, detection and power allocation for uplink user cooperation with NOMA and RSMA," *IEEE Trans. Wireless Commun.*, vol. 22, no. 1, pp. 471–485, Jan. 2023.

[16] H. Liu, Z. Bai, H. Lei, G. Pan, K. J. Kim, and T. A. Tsiftsis, "A new rate splitting strategy for uplink CR-NOMA systems," *IEEE Trans. Veh. Technol.*, vol. 71, no. 7, pp. 7947–7951, Jul. 2022.

[17] H. Liu, K. J. Kim, T. A. Tsiftsis, B. Clerckx, K. S. Kwak, and H. V. Poor, "Cognitive radio-inspired rate-splitting multiple access for semi-grant-free transmissions," *arXiv preprint arXiv:2208.07155*, 2022.

[18] Y. Xiao, S. A. Tegos, P. D. Diamantoulakis, Z. Ma, and G. K. Karagiannidis, "On the ergodic rate of cognitive radio inspired uplink multiple access," *IEEE Commun. Lett.*, vol. 27, no. 1, pp. 95–99, Jan. 2023.

[19] J. Park, B. Lee, J. Choi, H. Lee, N. Lee, S.-H. Park, K.-J. Lee, J. Choi, S. H. Chae, S.-W. Jeon *et al.*, "Rate-splitting multiple access for 6G networks: Ten promising scenarios and applications," *arXiv preprint arXiv:2306.12978*, 2023.

[20] A. Kumar, F. Y. Li, and J. Martinez-Bauset, "Revealing the benefits of rate-splitting multiple access for uplink IoT traffic," in *Proc. IEEE Global Commun. Conf. (GLOBECOM), Rio, Brazil*, Dec. 2022, pp. 111–116.

[21] E. J. Dos Santos, R. D. Souza, and J. L. Rebelatto, "Rate-splitting multiple access for URLLC uplink in physical layer network slicing with eMBB," *IEEE Access*, vol. 9, pp. 163 178–163 187, Dec. 2021.

[22] Y. Liu, B. Clerckx, and P. Popovski, "Network slicing for eMBB, URLLC, and mMTC: An uplink rate-splitting multiple access approach," *IEEE Trans. Wireless Commun.*, pp. 1–1, 2023.

[23] S. Bisen, P. Shaik, and V. Bhatia, "On performance of energy harvested cooperative NOMA under imperfect CSI and imperfect SIC," *IEEE Trans. Veh. Technol.*, vol. 70, no. 9, pp. 8993–9005, Sep. 2021.

[24] Z. Yang, Z. Ding, P. Fan, and G. K. Karagiannidis, "On the performance of non-orthogonal multiple access systems with partial channel information," *IEEE Trans. Commun.*, vol. 64, no. 2, pp. 654–667, Feb. 2016.

[25] C. Wang, T. C.-K. Liu, and X. Dong, "Impact of channel estimation error on the performance of amplify-and-forward two-way relaying," *IEEE Trans. Veh. Technol.*, vol. 61, no. 3, pp. 1197–1207, Mar. 2012.

[26] S. Singh and M. Bansal, "On the outage performance of uplink NOMA inspired CR network with CEEs and imperfect SIC," in *Proc. IEEE 6th Conf. Inf. and Commun. Tech. (CICT)*. IEEE, Nov. 2022, pp. 1–5.

[27] X. Chen, Z. Zhang, C. Zhong, R. Jia, and D. W. K. Ng, "Fully non-orthogonal communication for massive access," *IEEE Trans. Commun.*, vol. 66, no. 4, pp. 1717–1731, Apr. 2018.

[28] A. P. Chrysologou, N. D. Chatzidiamantis, and G. K. Karagiannidis, "Cooperative uplink NOMA in D2D communications," *IEEE Commun. Lett.*, vol. 26, no. 11, pp. 2567–2571, Nov. 2022.

[29] S. A. Tegos, P. D. Diamantoulakis, A. S. Lioumpas, P. G. Sarigiannidis, and G. K. Karagiannidis, "Slotted ALOHA with NOMA for the next generation IoT," *IEEE Trans. Commun.*, vol. 68, no. 10, pp. 6289–6301, Oct. 2020.

[30] J. Choi, "NOMA-based random access with multichannel ALOHA," *IEEE J. Sel. Areas Commun.*, vol. 35, no. 12, pp. 2736–2743, Dec. 2017.

[31] A. A. Tegos, S. A. Tegos, D. Tyrovolas, P. D. Diamantoulakis, P. Sarigiannidis, and G. K. Karagiannidis, "Breaking orthogonality in uplink with randomly deployed sources," *IEEE Open J. Commun. Soc.*, Jan. 2024.

[32] J. Che, Z. Zhang, Z. Yang, X. Chen, and C. Zhong, "Massive unsourced random access for NGMA: Architectures, opportunities, and challenges," *IEEE Network*, vol. 37, no. 1, pp. 28–35, 2023.

[33] I. Gradshteyn and I. Ryzhik, *Table of Integrals, Series, and Products*, 7th ed. New York, NY, USA: Academic, 2007.

[34] Y. Zhang, S. Feng, and W. Tang, "Performance analysis of hybrid cellular and bidirectional device-to-device cooperative NOMA communication systems," *IEEE Trans. Veh. Technol.*, vol. 70, no. 10, pp. 10 420–10 435, Oct. 2021.

This article has been accepted for publication in IEEE Transactions on Communications. This is the author's version which has not been fully edited and content may change prior to final publication. Citation information: DOI 10.1109/TCOMM.2024.3403502

Athanasios P. Chrysologou (Student Member, IEEE) was born in Thessaloniki, Greece. He received the Diploma degree in electrical and computer engineering from the Aristotle University of Thessaloniki, Greece, in 2021, where he is currently pursuing the Ph.D. degree with the Department of Electrical and Computer Engineering. His research interests include probability theory and multiple access in wireless communications. He was an Exemplary Reviewer of IEEE communications letters for 2022 (top 3% of reviewers).

Sotiris A. Tegos (Senior Member, IEEE) received the Diploma (5 years) and Ph.D. degrees from the Department of Electrical and Computer Engineering, Aristotle University of Thessaloniki, Thessaloniki, Greece, in 2017 and 2022, respectively. Since 2022, he is a Postdoctoral Fellow at the Wireless Communications and Information Processing (WCIP) Group, Aristotle University of Thessaloniki, Thessaloniki, Greece, and at the Department of Applied Informatics, University of Macedonia, Thessaloniki, Greece. Since 2023, he is also a Postdoctoral Fellow at the Department of Electrical and Computer Engineering, University of Western Macedonia, Kozani, Greece. In 2018, he was a visiting researcher at the Department of Electrical and Computer Engineering, Khalifa University, Abu Dhabi, UAE. His current research interests include multiple access in wireless communications, optical wireless communications, and reconfigurable intelligent surfaces. He is a Working Group Member of the Newfocus COST Action "European Network on Future Generation Optical Wireless Communication Technologies". He serves as an Editor for IEEE Communications Letters. He received the Best Paper Award in 2023 Photonics Global Conference (PGC). He was an exemplary reviewer in IEEE Wireless Communications Letters in 2019 and 2022 (top 3% of reviewers).

Panagiotis D. Diamantoulakis (Senior Member, IEEE) received the Diploma (5 years) and the Ph.D. degree from the Department of Electrical and Computer Engineering, Aristotle University of Thessaloniki, Thessaloniki, Greece, in 2012 and 2017, respectively. Since 2017, he is a Postdoctoral Fellow with Wireless Communications and Information Processing (WCIP) Group, AUTH and since 2021, he has been a Visiting Assistant Professor with the Key Lab of Information Coding and Transmission, Southwest Jiaotong University, Chengdu, China. Since 2022 he is also the Principal Investigator of a national research project, which is being implemented at the Department of Applied Informatics, University of Macedonia, Thessaloniki, Greece. His research interests include optimization theory and applications in wireless networks, optical wireless communications, and goal-oriented communications. He is a Working Group Member of the Newfocus COST Action "European Network on Future Generation Optical Wireless Communication Technologies." He serves as an Editor of IEEE Open Journal of the Communications Society, Physical Communications (Elsevier), and Frontiers in Communications and Networks, while during 2018-2023 he has been an Editor of IEEE Wireless Communications Letters. He was also an Exemplary Editor of the IEEE Wireless Communications Letters in 2020, and an Exemplary Reviewer of the IEEE Communications Letters in 2014 and the IEEE Transactions on Communications in 2017 and 2019 (top 3% of reviewers).

This article has been accepted for publication in IEEE Transactions on Communications. This is the author's version which has not been fully edited and content may change prior to final publication. Citation information: DOI 10.1109/TCOMM.2024.3403502

Nestor D. Chatzidiamantis (Member, IEEE) was born in Los Angeles, CA, USA, in 1981. He received the Diploma degree (5 years) in electrical and computer engineering (ECE) from the Aristotle University of Thessaloniki (AUTH), Greece, in 2005, the M.Sc. degree in telecommunication networks and software from the University of Surrey, U.K., in 2006, and the Ph.D. degree from the ECE Department, AUTH, in 2012. From 2012 through 2015, he worked as a Post-Doctoral Research Associate in AUTH and from 2016 to 2018, as a Senior Engineer at the Hellenic Electricity Distribution Network Operator (HEDNO). Since 2018, he has been Assistant Professor at the ECE Department of AUTH and member of the Telecommunications Laboratory. His research areas span signal processing techniques for communication systems, performance analysis of wireless communication systems over fading channels, communications theory, cognitive radio and free-space optical communications.

Paschalis C. Sofotasios (Senior Member, IEEE) was born in Volos, Magnesia, Greece. He received the M.Eng. degree from Newcastle University, U.K., the M.Sc. degree from the University of Surrey, U.K. and the Ph.D. degree from the University of Leeds, U.K. He has held academic positions with the University of Leeds, U.K., University of California at Los Angeles, CA, USA, Tampere University of Technology, Finland, Aristotle University of Thessaloniki, Greece and Khalifa University, UAE, where he is currently an Associate Professor with the Department of Communications and Computer Engineering. His research interests are in the broad field of physical layer digital and optical wireless communications. He received the Exemplary Reviewer Award from IEEE on Communications in 2015 and in 2016, the Best Paper Award at ICUFN 2013, and the Runner Up at IEEE ICT 2016 and IEEE Globecom 2018. He was the TPC Co-Chair of the Communication Theory Track of IEEE Globecom 2020 and he has served as an Editor at IEEE Communications Letters, from 2015 to 2019. Currently, he is an Editor in IEEE Transactions on Communications and an Editor-at-Large of the Communication Theory track in the IEEE Open Journal of the Communication Society.

George K. Karagiannidis (Fellow, IEEE) is currently Professor in the Electrical & Computer Engineering Dept. of Aristotle University of Thessaloniki, Greece and Head of Wireless Communications & Information Processing (WCIP) Group. He is also Faculty Fellow in the Cyber Security Systems and Applied AI Research Center, Lebanese American University. His research interests are in the areas of Wireless Communications Systems and Networks, Signal processing, Optical Wireless Communications, Wireless Power Transfer and Applications and Communications & Signal Processing for Biomedical Engineering. Dr. Karagiannidis was in the past Editor in several IEEE journals and from 2012 to 2015 he was the Editor-in Chief of IEEE Communications Letters. From September 2018 to June 2022 he served as Associate Editor-in Chief of IEEE Open Journal of Communications Society. Currently, he is the Editor-in-Chief of IEEE Transactions on Communications. Recently, he received three prestigious awards: The 2021 IEEE ComSoc RCC Technical Recognition Award, the 2018 IEEE ComSoc SPCE Technical Recognition Award and the 2022 Humboldt Research Award from Alexander von Humboldt Foundation. Dr. Karagiannidis is one of the highly-cited authors across all areas of Electrical Engineering, recognized from Clarivate Analytics as Highly-Cited Researcher in the nine consecutive years 2015-2023.